Eur. J. Mech. B/Fluids, **17**, n° 6, 875-900, 1998

Numerical and experimental investigation of thermal convection for a thermodependent Herschel-Bulkley fluid in an annular duct with rotating inner cylinder

C. NOUAR, C. DESAUBRY and H. ZENAIDI*

ABSTRACT. – Thermal convection for an incompressible Herschel-Bulkley fluid along an annular duct, whose inner cylinder is rotating and outer is at rest, is analyzed numerically and experimentally. The outer cylinder is heated at constant heat flux density and the inner one is assumed adiabatic. The first part of this study deals with the effect of the rheological behavior of the fluid and that of the rotation of the inner cylinder on the flow field and heat transfer coefficient. All the physical properties are assumed constant and the flow is assumed fully developed. The critical Rossby number $Ro_c = (R_1\,\Omega/U_d)_c$, for which the dimension of the plug flow is reduced to zero is determined with respect to the flow behavior index, the radius ratio and the Herschel-Bulkley number for axial flow. The rotation of the inner cylinder induces a decrease of the axial velocity gradient at the outer cylinder thereby reducing the heat transfer between the heated wall and the fluid. The second part of this study introduces the variation of the consistency K with temperature and analyzes the evolution of the flow pattern and heat transfer coefficient along the heating zone. Two cases are distinguished depending on the Rossby number: (i) $\mathrm{Ro} < \mathrm{Ro}_c$, the plug flow dimension increases along the heating zone; (ii) $\mathrm{Ro} < \mathrm{Ro}_c$, the decrease of K with temperature leads to the reappearance of the plug flow. For high angular velocities, it is possible to have a plug zone attached to the outer cylinder. Finally, a correlation is proposed for the Nusselt number. It shows clearly that the effect of thermodependency of K on the heat transfer becomes more important with increasing rotational velocity of the inner cylinder. © Elsevier, Paris.

1. Introduction

Heat exchangers with annular geometry are often used for thermal processing in industries such as food, chemical and petrochemical. This explains the numerous published studies of the thermal convection in this geometry. The major part of this work has been conducted for Newtonian fluids with different kinds of boundary conditions. However, the case of non-Newtonian fluids, particularly yield-stress fluids, has been less studied, despite their particular importance, in the food and pharmaceutical industries. Bird *et al.* (1983) gave a list of materials that fall into this category of fluids. Actually, the literature concerning heat transfer for yield stress fluids is still comparatively poor in experimental as well as in theoretical or numerical results. Naïmi *et al.* (1990) studied heat transfer experimentally for an aqueous solution of Carbopol 940 flowing in an annular duct with a rotating inner cylinder. The fluid is shear thinning and possesses a yield stress below which, it either will not flow, or will flow, as an unsheared plug. Its rheological behavior is described by a Herschel-Bulkley model with temperature-dependent consistency K. The relationship between the shear stress τ and the shear rate $\dot{\gamma}$ can be described in the case of unidirectional shear flow by: $\tau = \tau_s + K(T)|\dot{\gamma}|^n$ with $0 < n < 1$, where τ_s is the yield stress, n the flow behavior index, and $K(T)$ is a function of temperature. For fully developed Poiseuille flow and isothermal conditions, the flow field comprises a plug core moving as a rigid body, with viscoplastic shear regions adjacent to each cylinder. The rotation of the inner cylinder induces an orthoradial

* Laboratoire d'Énergétique et de Mécanique Théorique et Appliquée, C.N.R.S URA 875. 2, avenue de la Forêt de Haye, BP 160, 54054 Vandœuvre-lès-Nancy, France.
E-mail: cnouar@ensem.u-nancy.fr

0997-7546/98/06/© Elsevier, Paris

shear rate increasing the second invariant of the rate of deformation tensor. This leads to a reduction of the plug core dimension. Naïmi *et al.* (1990) set obviously, through axial velocity measurements, the disappearance of plug flow, for sufficiently high angular velocity of the inner cylinder. They did not give the critical angular velocity Ω_c for which the plug zone is reduced to zero. In fact, it is difficult to measure the plug dimension as a function of Ω. In the case where the annular gap can be approximated as a plane slot, Bittleston *et al.* (1992) presented for a Bingham fluid with an imposed axial pressure gradient, a simple expression of the critical rate at which the wall has to move to reduce the plug to zero.

As far as heat transfer is concerned, Naïmi *et al.* (1990) used an experimental setup, where the outer cylinder is heated at constant heat flux density ϕ_p, and the inner one is adiabatic. They determined the evolution of the local Nusselt number along the heating zone, from wall temperature measurements. Due to the decrease of K with temperature, they noted that: (i) the Nusselt number rises with increasing imposed heat flux; (ii) this rise is more important when the inner cylinder is rotating with a velocity such that the dimension of the plug core is reduced to zero. Finally, they presented the experimental results in the form of Nusselt number correlation. The effect of the variation of K with temperature on heat transfer is described by a dimensionless number $b\phi_p D_h/2\lambda : Nu \propto (b\phi_p D_h/2\lambda)^t$, where b is the temperature exponent of $K : K = a\exp(-bT)$. The exponent "t" is 0.1 for Poiseuille flow and 0.16, when the inner cylinder is rotating with a velocity such that the plug region is supressed. According to these authors, the plug region inhibits the development of radial velocity, and therefore limits the axial velocity deformation. Consequently, the thermodependency effect is reduced. These interesting results remain essentially qualitative. Furthermore, the preceding correlation was obtained for a particular fluid and a particular geometry.

Under the same work hypothesis as that of the previous authors, we analyze the thermal convection for a Herschel-Bulkley fluid, in an annular duct, with rotating inner cylinder numerically and experimentally. All the physical properties of the fluid are assumed to be constant except for the consistency. The present work has two main motivations. First, it seeks to provide a precise study of dynamical and thermal fields structure. Second, to determine Ω_c, and to attempt to arrive at a better comprehension and a better description of the effect of the variation of K with temperature on heat transfer.

In the first part, the flow is assumed fully developed, and K is independent of temperature. The critical angular velocity Ω_c is determined as a function of different dynamical, geometrical and rheological parameters. The analysis of the axial velocity gradient at the outer cylinder allows us to interpret the evolution of the heat transfer coefficient.

In the second part, we consider the case where K varies with temperature. We will be particularly interested in the evolution of the plug core edges, from the entrance section, when $\Omega < \Omega_c$. However, when $\Omega > \Omega_c$, the modification of the flow structure along the heating zone, due to the decrease of the consistency with temperature, leads to the reappearance of the plug flow between the two cylinders. The numerical results also show the possibility of a plug core attached to the outer cylinder. In the thermal entrance region, an asymptotic expression of the modification of the wall axial velocity gradient by the thermodependency of the consistency is proposed. It is obtained for high Péclet and Prandtl numbers. A large Péclet number allows us to make the lubrication approximation. A large Prandlt number allows us to consider that the dynamical relaxation length is very small compared with the thermal relaxation length. In the entry region, the temperature variations are small everywhere except in a very thin thermal boundary layer by the wall. As a result, viscosity variations are not sufficiently large to cause significant variation in the pressure gradient $(\partial p/\partial z)$. Therefore, the wall shear stress is assumed to be independent of z, that is the decrease of the apparent viscosity by the temperature, is balanced by the increase of the shear rate.

The plan of this paper is as follows: The experimental installation, instrumentation and test fluid are presented in §2. The problem is defined through the governing equations in §3. The procedure for obtaining numerical

solutions is described in §4. Experimental and numerical results are given and analyzed in §5. Finally, some conclusions are drawn in §6, about the effect of rotation of the inner cylinder, and of thermodependency of consistency on the dimension of the plug flow, and on the heat transfer between the outer cylinder and the fluid.

2. Experimental installation, instrumentation, test fluid

2.1. Experimental installation

- The experimental test were conducted in the same flow configuration as that described by Nouar *et al.* (1987) and Naïmi *et al.* (1990). Two test sections were used:

- The first aimed to characterize the flow structure, in an isothermal situation, by velocity measurements. It consists of two coaxial cylinders made of Plexiglass. The outer cylinder has an inner diameter of 65 mm, wall thickness of 45 mm and a length of 160 mm. The inner cylinder has a diameter of 40 mm and a length of 180 mm. The resulting annular space has a width and a length of 12.5 mm and 160 mm, respectively.

- The second test section is similar to the first one, and has the following characteristics:

*A Plexiglass inner cylinder of 40 mm diameter and 480 mm length.

*A copper outer cylinder with 65 mm inner diameter, 2.5 mm of thickness and 369 mm length, wrapped by a resistance loop. The whole system is insulated by an air gap enclosed by a Plexiglass shield.

The evolution of the outer cylinder wall temperature is determined by means of thirty one Chromel-Alumel thermocouples, placed at different axial positions on the wall. At 16.5 mm before the end of the heating zone, four thermocouples were placed circumferentially, 90° apart, in order to examine the axisymmetry of the thermal field. The fluid temperature T_e, at the inlet of the heated test section, was also measured by a Chromel-Alumel thermocouple, and maintained constant within a tolerance of 0.1°C, during each experimental test.

The rotational velocity of the inner cylinder is determined by means of an opto-electronic sensor, linked to a frequency-meter. The maximum error in the angular velocity of the inner cylinder is estimated at 0.1 rad/s. The velocity measurements are performed using a Laser Doppler Velocity system from DISA. It comprises a 35 mW helium-neon laser with a focusing lens to form the control volume in the test section. The principal characteristics of the optical system are given in Table 1. The light scattered by particles passing through this volume is collected in the photomultiplier and processed by a Doppler frequency tracker.

Table I. – Characteristics of optical arrangement.

Focal length of the focusing lens (mm)	120
Half angle of the beam interaction (degrees)	10.62
Fringe spacing (μm)	1.73
Number of fringes	52
Diameter of the control volume at $1/e^2$ intensity in air (μm)	90
Length of the control volume at $1/e^2$ intensity in air (μm)	500
Frequency to velocity conversion (ms^{-1}/MHz)	1.7168

2.2. Test fluid

The fluid used is an aqueous gel of an acrylic acid polymer (Carbopol 940). It is prepared by dissolving the polymer powder (hygroscopic white powder) in demineralized water, and then, raising the Ph value until neutralization. The weight concentration of Carbopol is 0.2%. A small amount of preservative (formaldehyde) was added in order to limit bacterial contamination. The neutralization of the Carbopol 940 is accompanied

by a gelation process. According to Alain (1973), this transition is due to unfolding of the long polymer chain, and is only due to the effect of overcrowding and tangling of the spreaded chains to which the gel is going to be structured.

The cone and plate geometry of a Carrimed (CS-100) constant torque rheometer was used in order to study the rheological behavior of the working fluid. The rheograms were determined at different temperatures ranging from 10°C to 60°C. The curves fitting $\tau(\dot{\gamma})$ indicate that the rheological behavior of the solution can be described by the Herschel-Bulkley relation: $\tau = \tau_s + k\dot{\gamma}^n$, in the range of shear rates from 0.7 to about 600 s^{-1}. The determination of the yield stress requires some care since it could be linked to the sensitivity of the device. According to Magnin and Piau (1987), a slip flow can appear at low values of the shear rate. In our experimental tests, the wall shear rate is enough to avoid slipping, and the rheological parameters have been determined on the range of shear rate that offers the best correlation coefficient (≈ 0.999) for a Herschel-Bulkley law. This is acceptable since the heat transfer is governed by the wall shear rate. The evolution of the behavior law, when the shear rate tends to zero, has practically no effect on the velocity profile.

Figure 1 shows, on semi-logarithmic coordinates, the evolution of the yield stress, the consistency K and the flow behavior index n as a function of temperature. It appears that the temperature dependence of τ_s and n are weak, compared to the temperature dependence of K, and thus can be ignored. The relation $K - T$ adopted is $K = K_0 \exp(-bT)$. A possible explanation of the weak dependence of τ_s on temperature (Forrest and Wilkinson, 1973) is that the yield stress is mainly dependent on a mechanical locking of the fluid, which is essentially temperature independent. The rheological behavior is described by $\tau = 32 + 16\exp(-0.014T)\dot{\gamma}^{0.43}$. The fluid considered in Figure 1 was prepared three weeks before the corresponding rheometric test. Its rheological behavior, just after the preparation is given by $\tau = 41 + 42.0\exp(-0.012T)\dot{\gamma}^{0.34}$. The fluid ages and deteriorates gradually because of thermal and mechanical constraints that it undergoes in the experimental device. Therefore, the analysis of the rheological behavior of the fluid was studied after each experimental run.

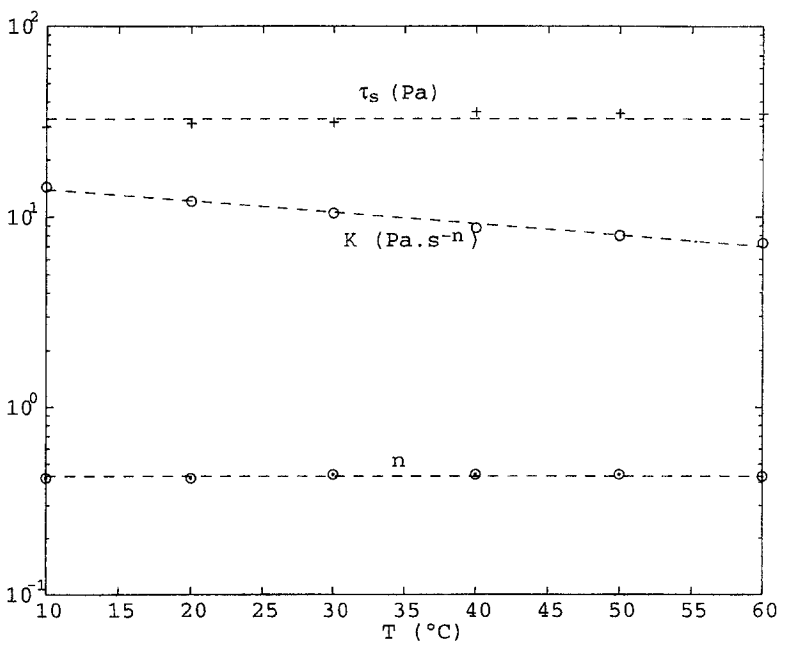

Fig. 1. – Evolution of the rheological parameters τ_s, n and K as a function of temperature.

The thermal conductivity λ and the specific heat Cp are assumed to be that of the water solvent, since the concentration of Carbopol is very low.

3. Basic equations

The fluid is assumed incompressible and thermodependent only by its consistency K. The flow is assumed steady, laminar and axisymmetric. At the entrance of the heated region ($z = 0$), the flow is fully developed and the fluid temperature T_e is constant and uniform. The coordinate system, the axial, radial and tangential components of the velocity are shown on Figure 2. The following dimensionless quantities are introduced:

$$\eta = \frac{r}{R_2};\ Z = \frac{z}{L};\ U = \frac{u}{U_d};\ V = \frac{v}{U_d R_2/L};\ W = \frac{w}{U_d};\ P = \frac{p}{\rho U_d^2}$$

$$N = \frac{R_1}{R_2};\ \overline{\mu}_a = \frac{\mu_a}{\mu_0};\quad \Delta\Theta = \frac{\Delta T}{\phi_p(R_2 - R_1)/\lambda}.$$

μ_a is the apparent viscosity of the fluid calculated at the local temperature T; μ_0 corresponds to the apparent viscosity calculated at the inlet temperature T_e, and at the outer cylinder wall shear rate, for a fully developed Poiseuille flow; ϕ_p is the heat flux density, U_d is the mean axial velocity, and L is a typical axial scale length of temperature variations, given by $L = \rho Cp\, U_d\,(R_2 - R_1)^2/\lambda$. It can be viewed as a length over which downstream convection balances transverse conduction. $2L/(R_2 - R_1)$ is the Péclet number.

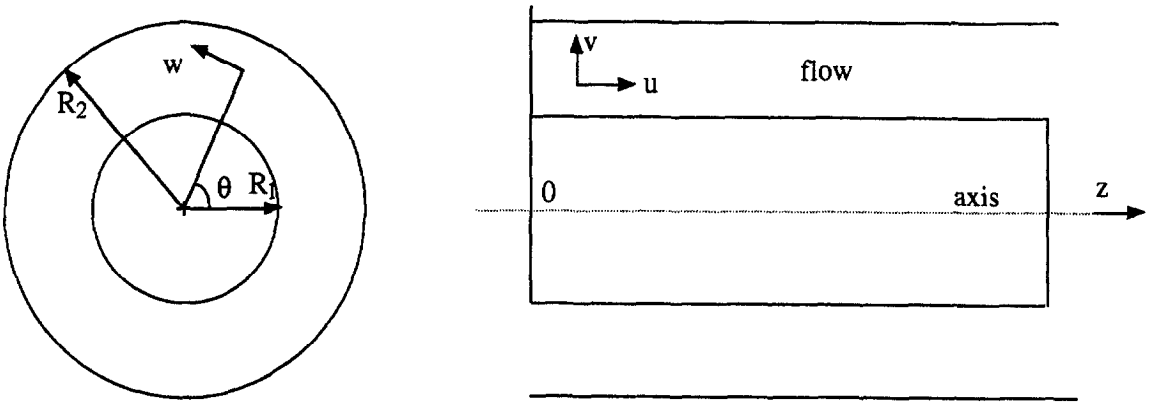

Fig. 2. – System of coordinates.

The governing equations of the problem are:

– continuity equation:

$$\frac{\partial}{\partial Z}(\eta U) + \frac{\partial}{\partial \eta}(\eta V) = 0, \tag{1}$$

– tangential momentum equation:

$$\left[U\frac{\partial W}{\partial Z} + V\frac{\partial W}{\partial \eta} + \frac{VW}{\eta}\right] = \frac{\mathrm{Pr}(1-N)^2}{\eta^2}\frac{\partial}{\partial \eta}\left[\eta^2 \overline{\mu}_a\left(\frac{\partial W}{\partial \eta} - \frac{W}{\eta}\right)\right] + \frac{4}{\mathrm{RePe}}\frac{\partial}{\partial Z}\left[\overline{\mu}_a \frac{\partial W}{\partial Z}\right], \tag{2}$$

– radial momentum equation:

$$\frac{4}{(1-N)^2\mathrm{Pe}^2}\left[V\frac{\partial V}{\partial \eta}+U\frac{\partial V}{\partial Z}\right]-\frac{W^2}{\eta}=-\frac{\partial P}{\partial \eta}+\frac{8}{\mathrm{RePe}}\frac{1}{\eta}\frac{\partial}{\partial \eta}\left[\eta\overline{\mu}_a\frac{\partial V}{\partial \eta}\right]-\frac{8}{\mathrm{RePe}}\frac{V}{\eta^2}+\frac{4}{\mathrm{RePe}}\frac{\partial}{\partial Z}\left[\overline{\mu}_a\frac{\partial U}{\partial \eta}\right]+\frac{16}{(1-N)^2}\frac{1}{\mathrm{Pe}^3\mathrm{Re}}\frac{\partial}{\partial Z}\left[\overline{\mu}_a\frac{\partial V}{\partial \eta}\right], \tag{3}$$

– axial momentum equation:

$$\left[U\frac{\partial U}{\partial Z}+V\frac{\partial U}{\partial \eta}\right]=-\frac{\partial P}{\partial Z}+\frac{Pr(1-N)^2}{\eta}\frac{\partial}{\partial \eta}\left[\eta\overline{\mu}_a\frac{\partial U}{\partial \eta}\right]+\frac{4}{\mathrm{RePe}}\frac{1}{\eta}\frac{\partial}{\partial \eta}\left[\eta\overline{\mu}_a\frac{\partial V}{\partial Z}\right]+\frac{8}{\mathrm{RePe}}\frac{\partial}{\partial Z}\left[\overline{\mu}_a\frac{\partial U}{\partial Z}\right]. \tag{4}$$

– continuity equation in integral form:

$$\int_N^1 \eta U\,d\eta=\frac{(1-N^2)}{2}, \tag{5}$$

– energy equation:

$$U\frac{\partial \Theta}{\partial Z}+V\frac{\partial \Theta}{\partial \eta}=\frac{(1-N)^2}{\eta}\frac{\partial}{\partial \eta}\left[\eta\frac{\partial \Theta}{\partial \eta}\right]+\frac{4}{\mathrm{Pe}^2}\frac{\partial}{\partial Z}\left[\frac{\partial \Theta}{\partial Z}\right]+\mathrm{Br}\,\overline{\mu}_a\left[\left(\frac{\partial U}{\partial \eta}\right)^2+\left(\eta\frac{\partial}{\partial \eta}\left(\frac{\partial W}{\partial \eta}\right)\right)^2\right], \tag{6}$$

where Pr, Re and Br are respectively the Prandtl number, Reynolds number and Brinkman number. They are defined by:

$$\mathrm{Pr}=\mu_0 Cp/\lambda;\ \mathrm{Re}=2\rho U_d(R_2-R_1)/\mu_0;\ \mathrm{Br}=\mu_0 U_d^2(1-N)^2/\phi_p(R_2-R_1).$$

In this study, Br is very small and can eventually be neglected. Furthermore, the Péclet number is sufficiently high ($\mathrm{Pe}>100$) so that the axial convection dominates the axial conduction. Hence, all the terms of $0(1/\mathrm{Pe}^{\alpha}, \alpha \geq 1)$ as the axial diffusion term, are neglected.

– Rheological behavior:

The constitutive equation uses the Von Mises yield condition. It is given by:

$$\bar{\bar{\tau}}=2\mu_a\bar{\bar{D}} \quad \text{if} \quad (\tau_{II})^{1/2}>\tau_s \tag{7-a}$$

and

$$\bar{\bar{D}}=0 \quad \text{if} \quad (\tau_{II})^{1/2}\leq\tau_s \tag{7-b}$$

where $\bar{\bar{\tau}} = \bar{\bar{\Sigma}} + p\,\bar{\bar{1}}$ and $\bar{\bar{D}}$ are the deviatoric extra-stress and rate of deformation tensors, p is the pressure, $\bar{\bar{\Sigma}}$ the stress tensor and τ_s the yield stress. Scalars D_{II} and τ_{II} are the second invariant of tensors $\bar{\bar{D}}$ and $\bar{\bar{\Sigma}}$, respectively:

$$D_{II} = (1/2)\mathrm{tr}\bar{\bar{D}}^2 \quad \text{and} \quad \tau_{II} = (1/2)\mathrm{tr}\bar{\bar{\tau}}^2.$$

The apparent viscosity μ_a is given by:

$$\mu_a = K\,(4D_{II})^{(n-1)/2} + \tau_s(4D_{II})^{-1/2}. \tag{8}$$

The expression of the second invariant D_{II}, in terms of velocity derivatives is:

$$D_{II} = \frac{1}{4}\left[\left(\frac{\partial w}{\partial r} - \frac{w}{r}\right)^2 + \left(\frac{\partial u}{\partial r}\right)^2\right] + \frac{1}{2}\left[\left(\frac{\partial v}{\partial r}\right)^2 + \left(\frac{v}{r}\right)^2\right]. \tag{9}$$

Equations (7-a and 7-b) define two distinct flow regions. In the first, the invariant τ_{II} exceeds the yield stress, and the material flows with a non-Newtonian viscosity μ_a, given by equation (8). In the second, the stress is less than the yield value, and the material behaves as a rigid solid. The surface $\tau_{II} = (1/2)tr\,\bar{\bar{\tau}}^2$ marks the boundary between the shearing fluid and fluid that is either at rest or moving with a uniform velocity.

The boundary conditions for U, V, W and Θ are:

$$\begin{aligned} &U(\eta, Z=0) = U_{cd}(\eta);\ W(\eta, Z=0) = W_{cd}(\eta) \\ &V(\eta, Z=0) = 0;\ \Theta(\eta, Z=0) = \Theta_e, \end{aligned} \tag{10}$$

$$U(\eta = N, Z) = V(\eta = N, Z) = 0;\ W(\eta = N, Z) = \frac{R_1\Omega}{U_d};\ \frac{\partial\Theta}{\partial\eta}(\eta = N, Z) = 0 \tag{11}$$

and

$$U(\eta = 1, Z) = V(\eta = 1, Z) = W(\eta = 1, Z) = 0;\ \frac{\partial\Theta}{\partial\eta}(\eta = 1, Z) = \frac{1}{1-N} \tag{12}$$

where:

U_{cd}, W_{cd} and Θ_e are the fully developed axial and tangential velocities and the inlet uniform temperature respectively and ϕ_p is the heat flux density at the wall of the outer cylinder. The dimensionless number $R_1\Omega/U_d$ is the Rossby number, it will be denoted by Ro.

4. Numerical solution

Equations (7-a) and (7-b) hold in different regions of the flow, whose locations are not known a priori. This is one of the major difficulties in obtaining a numerical solution. An additional difficulty results in the singularity in (8) as $D_{II} \to 0$, *i.e.* as the yield surface is approached. To overcome these difficulties, a modified version of the rheological equation is used. The modified equation is continuous and applies in both the yielded and unyielded zones, thereby eliminating the problem of having to find the yield surfaces, before calculating the velocity field. Here, we follow the approach adopted by several authors, notably (Bercovier and Engelman, 1980) and (Beris *et al.*, 1985) in replacing the magnitude of the strain rate tensor $(4D_{II})^{1/2}$ by $(4D_{II})^{1/2} + \varepsilon$,

in (8). Here, ε is a small regularization parameter, with dimensions of strain rate. The modified rheological equation is then given by:

$$\mu_a = K[(4D_{II})^{1/2} + \varepsilon]^{n-1} + \tau_s/((4D_{II})^{1/2} + \varepsilon) \tag{13}$$

To track down the location of the yield surface, we employ the criterion that the material flows only when the magnitude of the extra stress tensor exceeds the yield stress. Thus, the location of the yield stress surface corresponds to $1/2\,\tau : \tau = \tau_s^2$. For small values of ε, the second invariant of the rate of strain tensor at the yield surface will be $(4D_{II}) \approx (\tau_s\varepsilon/K)^{2/(1+n)}$. So the unsheared zone will have strain rates of $O[(\tau_s\varepsilon/K)^{1/(1+n)}]$ or less, and therefore consists of a highly viscous fluid, rather than a rigid solid.

Equations (1)-(6), (13) as well as the associated boundary conditions are solved by means of an extension to the linearized implicit finite difference technique of El-Shaarawi *et al.* (1982). The product terms of the momentum equation are linearized, by setting the unknown to its value at the previous axial step. A second-order central difference scheme is employed, in approximating all partial derivatives in the radial direction, and the upwind scheme is used for the convective axial term. The integral representation of the continuity equation is determined by the trapezoidal rule. After some modifications, the discretized equations lead to a system of tridiagonal matrices, which are solved by the Thomas algorithm. The momentum and energy equations are parabolic in the streamwise direction. The solution is then marched from the entrance section to the final station.

As far as the consistency and the stability of the resultant finite difference equations are concerned, we show by extending the technique of El-Shaarawi *et al.* (1982) that they are consistent representation of equations (1)-(5). They are also stable for all mesh sizes, as long as the downstream axial velocity is positive, *i.e.*, as long as no flow reversal occurs within the domain of solution.

The regularization parameter must be sufficiently small, in order to describe the rheological behavior of a Herschel-Bulkley material, but without creating numerical difficulties due to too abrupt changes in the viscosity near the yield point. Here, the regularization parameter was chosen so that on three lower decades ($\varepsilon/10$, $\varepsilon/100$ and $\varepsilon/1000$), the relative variation of the pressure gradient, and of the plug zone dimension (when it is not zero), remains less than 1%. As an example, Figure 3 shows, for an isothermal situation, the dependence of the plug zone dimension on the regularization parameter ε for $N = R_1/R_2 = 0.5$, $n = 0.5$, $ap_0 = 0.5$ and $\mathrm{Ro} = 1$, where ap_0 is the ratio of the plug width to the annular gap, when $\Omega = 0$. Results indicate for this case, that $\varepsilon = 5.10^{-6}$ satisfies the imposed criterion. We find that if the regularization parameter ε is set to too small value, then the number of iterations increases, and consequently, the roundoff errors also.

The accuracy of the numerical solution was investigated, by refining the grid in the radial and axial directions. As an example, Figure 4, gives the plug zone dimension, as a function of the number of nodes between the cylinders, for an isothermal situation and established dynamical regime. One observes that, from 1000 nodes, the solution is independent of the grid system. Verifications have been undertaken for different values of ap_0. Actually, the convergence based on the pressure gradient needs less nodes (200 nodes). In this paper, a very fine regular grid (2000 nodes) in the radial direction was used. The grid size, in the z direction, is very fine near the entrance section (a dimensionless axial mesh size $\Delta Z = 2.0\,10^{-6}$ ($\approx 0.5\,\mathrm{mm}$) was used), and coarser downstream.

5. Results and discussion

5.1. Temperature-independent consistency

The flow structure, for an established dynamic regime, can be obtained by solving numerically the system of equations (2)-(4) simplified, since the flow is translational invariant along Z and $V = 0$. As the apparent

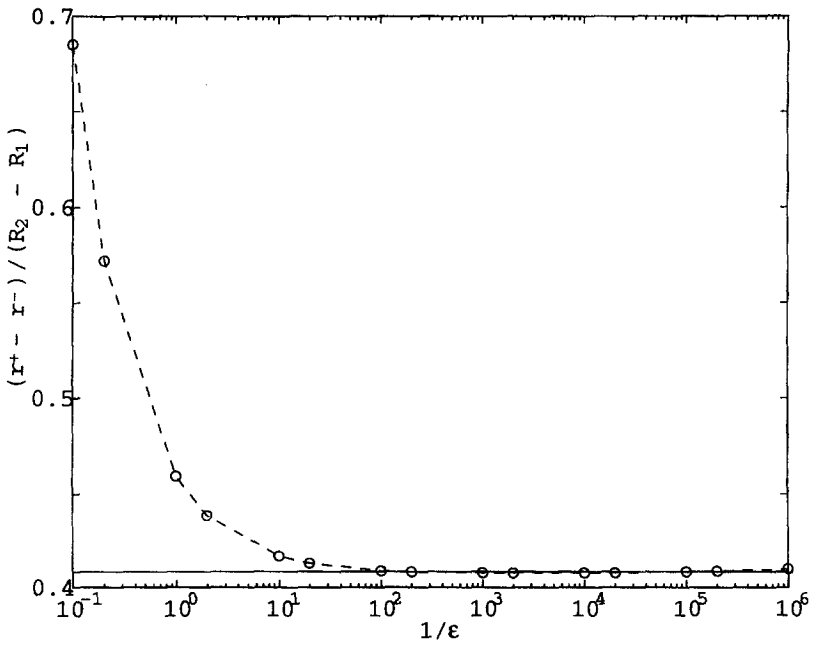

Fig. 3. – Dependence of the plug zone dimension on the value of the regularization parameter ε : $n = 0.5$; $ap_0 = 0.5$; $N = 0.5$; Ro $= 1.0$; (____) extension of Bittleston and Hassager (1992) method.

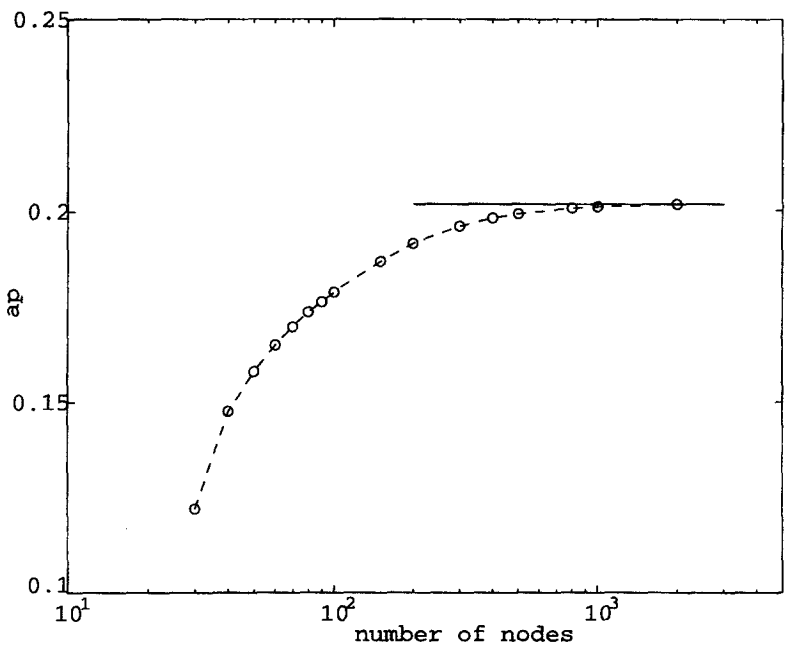

Fig. 4. – Relative dimension of the plug flow versus number of grid points in the radial direction . $ap_0 = 0.28$; $n = 0.5$; $N = 0.603$; Ro $= 0.56$; $\varepsilon = 5.10^{-6}$: (____) extension of Bittleston and Hassager (1992) method.

viscosity depends on the velocity gradients, an iterative process has been adopted. An initial known viscosity profile, for example, that of Poiseuille flow is assumed. The velocities U and W are then calculated and used to update the apparent viscosity. This procedure is repeated until the following norm is less than 10^{-5}

$$\text{norm}\, U = \text{Max}\left[\frac{|U^k - U^{k-1}|}{U^{k-1}}\right]_{N<\eta<1} \equiv \text{norm}\, W$$

where k is the iteration number.

Remark 1. – The flow structure for an established dynamic regime does not depend on the thermophysical properties of the fluid. The fact that Pr appears in the radial diffusion term of the axial momentum equation is an artefact of the chosen axial length scale. Actually, Pr can be simplified easily since $Z = 2z/[(R_2 - R_1)\text{RePr}]$.

In order to validate the results obtained by the regularized method, another procedure, where the plug is a rigid solid, was developed. It is an extension of that proposed by Bittleston and Hassager (1992), for a specified pressure gradient. Moreover, it uses a similar numerical algorithm. Figure 3 is an example of validation. The dimension of the plug zone, calculated by the second method, is practically identical to that obtained by the first one.

In this part of the study, we consider also the case where the gap between the two cylinders is small, compared to the mean radius. It is equivalent, at least to a first approximation, to neglecting the effect of curvature, and treating the annulus as a slot.

5.1.1. *Dimension of the plug flow*

The relative dimension ap of the plug zone, the Herschel-Bulkley numbers Hb_a and Hb_r, for axial and rotational flows, are respectively defined by:

$$ap = \frac{r^+ - r^-}{R_2 - R_1};\quad \text{Hb}_a = \frac{\tau_s}{K\left[\frac{U_d}{R_2 - R_1}\right]^n} \quad \text{and} \quad \text{Hb}_r = \frac{\tau_s}{K\left[\frac{R_1\Omega}{R_2 - R_1}\right]^n}$$

r^+ and r^- are respectively the internal and external radii of the plug zone.

In the case of Poiseuille flow, there is a detached moving plug of unyielded fluid between the two coaxial cylinders. Based on the works of Fordham *et al.* (1991) and of Bird *et al.* (1983), Nouar *et al.* (1996) presented diagrams which allow the determination of the plug core dimension ap_0, as well as its position, in the annular space, as a function of the flow behavior index n, the radius ratio N and of the Herschel-Bulkley number Hb_a. From these diagrams, one can see that ap_0 increases with Hb_a. So: (i) for a given rheological and geometrical parameters, the dimension of the plug flow decreases with the axial flow rate (but it is never zero) and (ii) ap_0 increases when the consistency decreases.

In the case of Couette flow, it is known that, for low angular velocity Ω of the inner cylinder, there is a flow near the inner cylinder and a stationary plug of unyielded fluid attached to the outer cylinder. When Ω is large, say $\Omega > \overline{\Omega}$, there is flow in the entire annular space. Simple calculations show that $\overline{\Omega}$ satisfies:

$$\overline{\text{Hb}}_r = \frac{\tau_s}{K(R_1\overline{\Omega}/(R_2 - R_1))^n} = \left[\frac{1-N}{N}\right]^n \left[\int_N^1 \frac{1}{\eta}\left[\frac{1}{\eta^2} - 1\right]^{1/n} d\eta\right]^{-n}$$

What happened in the Couette-Poiseuille flow? As we will show, the interaction of the various possible plug regions described above, is not immediately obvious. The application of the π-theorem leads to:

$$ap = f\,(N, n, \text{Hb}_a, \text{Ro});\quad \text{Ro} = \frac{R_1\Omega}{U_d}.$$

For Poiseuille flow:

$$ap_0 = f(N, n, \text{Hb}_a).$$

The diagrams obtained by Nouar *et al.* (1996), indicate that for a given N and n, the function f is bijective. We can then write:

$$ap = f(N, n, ap_0, \mathrm{Ro})$$

The critical Rossby number Ro_c from which the plug zone ap is reduced to zero, is such that:

$$\mathrm{Ro}_c = f\,(N, n, ap_0)$$

Figure 5 gives in a semi-logarithmic coordinates, the critical Rossby number as a function of ap_0, for $n = 0.5$ and seven values of the radius ratio N, from 0.2 to 0.8. For a specified N and U_d, the critical angular velocity increases with ap_0. The change of curvature observed for the different curves corresponds to values of ap_0 for which the inner cylinder rotation induces a strong modification of the flow structure. This point will be discussed in §5.1.2 and 5.1.3. Figure 5 shows also, that as the gap is larger, Ro_c becomes more important. A continuous line represents the curve for the slot approximation. The effect of the flow behavior index on Ro_c, was studied for two values of ap_0 : 0.3 et 0.5, and two radius ratios 0.4 and 0.6. The numerical results show a weak influence of n for $0.3 \leq n \leq 0.8$.

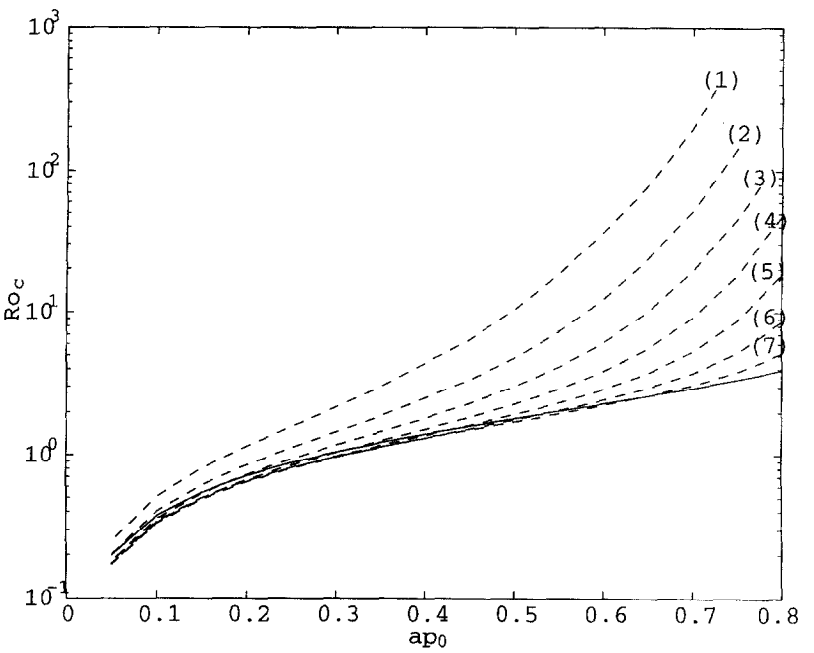

Fig. 5. – Evolution of Ro_c as a function of ap_0 for $n = 0.5$ and different radius ratios. (1) $N = 0.2$; (2) $N = 0.3$; (3) $N = 0.4$; (4) $N = 0.5$; (5) $N = 0.6$; (6) $N = 0.7$; (7) $N = 0.8$; (____) slot approximation.

Figure 6a shows how the width of the plug region is diminished with increasing rotation rate. It gives ap/ap_0 as a function of $\mathrm{Ro}/\mathrm{Ro}_c$, for $N = 0.5$, $n = 0.5$ and five values of ap_0 : 0.2; 0.4; 0.6; 0.7; and 0.8. When $\mathrm{Ro} = 0$; $ap = ap_0$, then ap decreases until it cancels out for $\mathrm{Ro} = \mathrm{Ro}_c$. For a given $\mathrm{Ro}/\mathrm{Ro}_c$, the decrease of ap/ap_0 is more rapid with increasing ap_0. The evolution of the internal (-) and external (+) radii of the plug zone, as a function of $\mathrm{Ro}/\mathrm{Ro}_c$, is represented in Figure 6b. It shows that for a low value of ap_0, the plug zone is reduced practically in the same way from external and internal edges. On the other hand, for large ap_0, the plug zone is reduced essentially from the internal edge, and the external one evolves slowly with $\mathrm{Ro}/\mathrm{Ro}_c$.

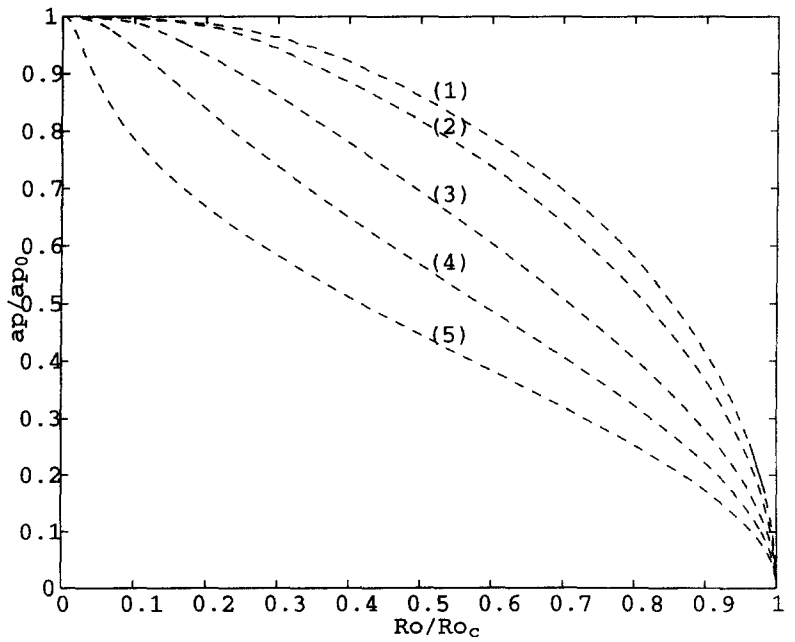

(a)

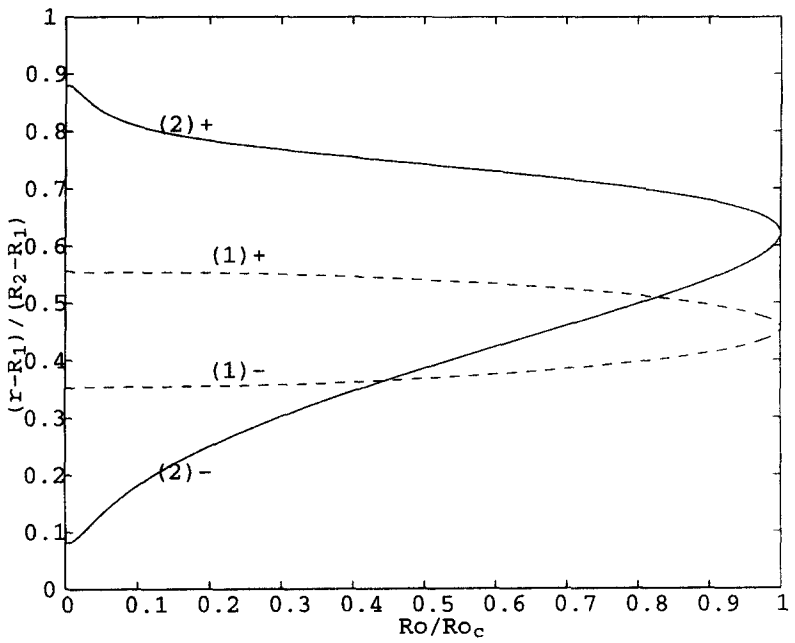

(b)

Fig. 6. – a) Evolution of the ratio of the plug flow dimension ∂p to that obtained for Poiseuille flow ap_0, against $\mathrm{Ro}/\mathrm{Ro}_c$: $N = 0.5$; $n = 0.5$. (1) $ap_0 = 0.2$; (2) $ap_0 = 0.4$; (3) $ap_0 = 0.6$; (4) $ap_0 = 0.7$; (5) $ap_0 = 0.8$; b) Radial position of the internal (–) and external (+) edges of the plug flow as a function of $\mathrm{Ro}/\mathrm{Ro}_c$: $N = 0.5$; $n = 0.5$; (1) $ap_0 = 0.2$; (2) $ap_0 = 0.8$.

5.1.2. *Axial velocity profiles*

The inner cylinder rotation induces a modification of the axial velocity profile, characterized by a decrease of $(\partial u/\partial r)$, at the wall of the outer cylinder. This deformation is due to a decrease of the apparent viscosity in the vicinity of the inner cylinder, where shear rate increases due to rotation. This result is illustrated in

Figure 7a, where we have represented three axial velocity profiles, corresponding to Poiseuille flow (curve 1), and Couette-Poiseuille flow for two angular velocities (13.8 ± 0.1) rad/s (curve 2) and (28.1 ± 0.1) rad/s (curve 3). The corresponding Rossby numbers are 3.8 and 7.7 respectively. The flow rate is practically the same for the three tests: $Qv = (1.50 \pm 0.03)10^{-4}\,\mathrm{m}^3/\mathrm{s}$. The velocity profiles were measured at a distance of 0.11 m from the inlet. According to Round (1993), this distance is sufficient for the development of the dynamic regime. The rotational velocities given above are such that the corresponding Taylor number is less than the critical value, at which Taylor vortices occur. Our assumptions are based on the stability diagram of Naïmi *et al.* (1990), obtained via flow visualization experiments.

The critical Rossby number calculated from the rheological parameters is 0.65. The disappearance of the plug core (for $\mathrm{Ro} > \mathrm{Ro}_c$) is clearly shown by curves 2 and 3. The theoretical profiles are represented by continuous line. For the three curves, a maximum deviation of 5% between the experimental profiles and the theoretical ones is observed. The theoretical dimension of the plug region, for Poiseuille flow is of 0.22 and is marked by broken lines. The axial velocity profile obtained for $\mathrm{Ro} = \mathrm{Ro}_c$ departs weakly from that of Poiseuille flow, and therefore was not represented. Figure 7b shows three numerical axial velocity profiles, obtained for $N = 0.5$, $ap_0 = 0.8$, $n = 0.5$ and $\mathrm{Ro}/\mathrm{Ro}_c = 0$; 0.5 and 1. The maximum axial velocity is not that of the plug when the inner cylinder is rotating: this is what we have called "strong modification of the flow structure", in §5.1.1.

5.1.3. *Tangential velocity profiles*

One should note that, inside a plug, the tangential velocity increases linearly with radial position. The analysis of the tangential velocity profiles, makes it possible to examine the axial flow effect on the rotational one, and to demonstrate complementary information concerning the evolution of the plug flow dimension, as a function of Ro. Figure 8 a shows three tangential velocity profiles, obtained for the following parameters: Curve 1: $\Omega = (2.75 \pm 0.1)$ rad/s, $Qv = (1.50 \pm 0.03)10^{-4}\,\mathrm{m}^3/\mathrm{s}$, $ap_0 = 0.24$ and $\mathrm{Ro}/\mathrm{Ro}_c = 1.01$. This corresponds to the situation where the plug core is reduced to zero, in the same way from the external and internal edges. Though the plug zone was reduced to zero, the tangential velocity still evolves practically linearly in the central part of the annular space. Curve 2: $\Omega = (13.8 \pm 0.1)$ rad/s, $Qv = (1.50 \pm 0.03)10^{-4}\,\mathrm{m}^3/\mathrm{s}$, $ap_0 = 0.24$ and $\mathrm{Ro}/\mathrm{Ro}_c = 5.1$. Curve 3: $\Omega = (13.8 \pm 0.1)$ rad/s and $Qv = 0$. This latter situation corresponds to pure Couette flow, without unyielded fluid ($\overline{\Omega} = 1.4\,\mathrm{rad/s}$). The profiles 2 and 3 are practically identical in the proximity of the inner cylinder, where the tangential flow is dominating. When one leaves the vicinity of the inner cylinder wall, profile 2 shows that the axial flow induces an increase of the tangential velocity, compared to the case of pure Couette flow.

Figure 8b shows numerical tangential velocity profiles for $\mathrm{Ro}/\mathrm{Ro}_c = 1$, and for two values of ap_0 : 0.2 and 0.8. For this latter value, the tangential flow is concentrated essentially near the inner cylinder. Consequently, the plug is reduced essentially from its inner edge, as it was observed in Figure 6b (curve 2).

5.1.4. *Heat transfer*

The heat transfer between the heated wall and the fluid depends on the wall axial velocity gradient $(\partial u/\partial r)_{r=R_2}$. For a Newtonian fluid, the evolution of the Nusselt number as a function of X^+ in the thermal inlet region of an annular duct was given by Worsoe-Schmidt (1967) as:

$$\mathrm{Nu}_{\mathrm{Newt}} = \frac{\phi_p D_h}{\lambda(T_p - T_m)} = 1.034(1-N)^{1/3}\varphi_p^{1/3}(X^+)^{-1/3} \tag{14}$$

Where: T_p and T_m are the wall and the bulk temperatures; X^+ is the Cameron number: $X^+ = Z/2$ and $\varphi_p = \partial(u/U_d)/\partial(r/R_2)$ is a dimensionless axial velocity gradient, calculated at the heated wall.

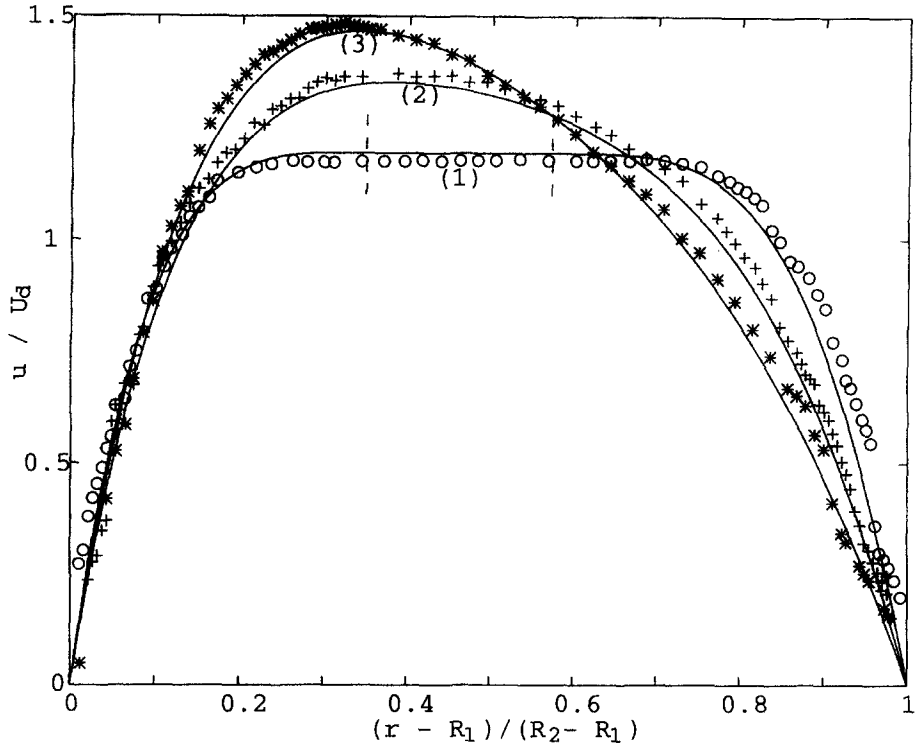

(a)

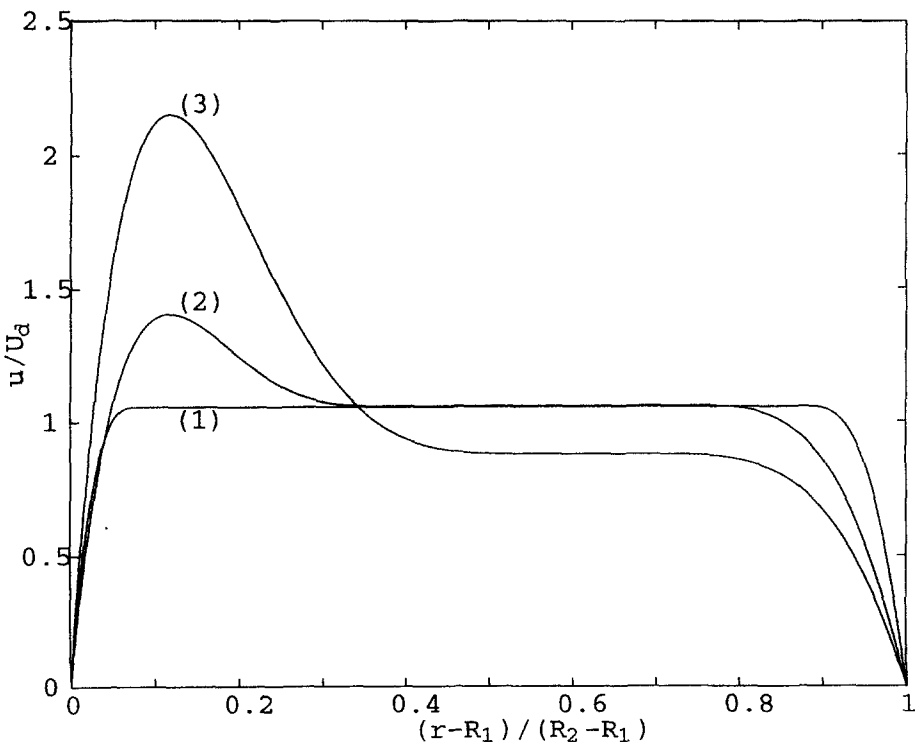

(b)

Fig. 7. – a) Fully developed axial velocity. (____) numerical; $Qv = 1.5\,10^{-4}$ m^3/s: $\Omega_c = 2.38$rd/s; (1) $\Omega = 0$; (2) $\Omega/\Omega_c = 5.8$;(3) $\Omega/\Omega_c = 11.80$; b) Fully developed axial velocity profiles: $n = 0.5$; $ap_0 = 0.8$; $N = 0.5$ (1) $\mathrm{Ro}/\mathrm{Ro}_c = 0$; (2) $\mathrm{Ro}/\mathrm{Ro}_c = 0.5$; (3) $\mathrm{Ro}/\mathrm{Ro}_c = 1$.

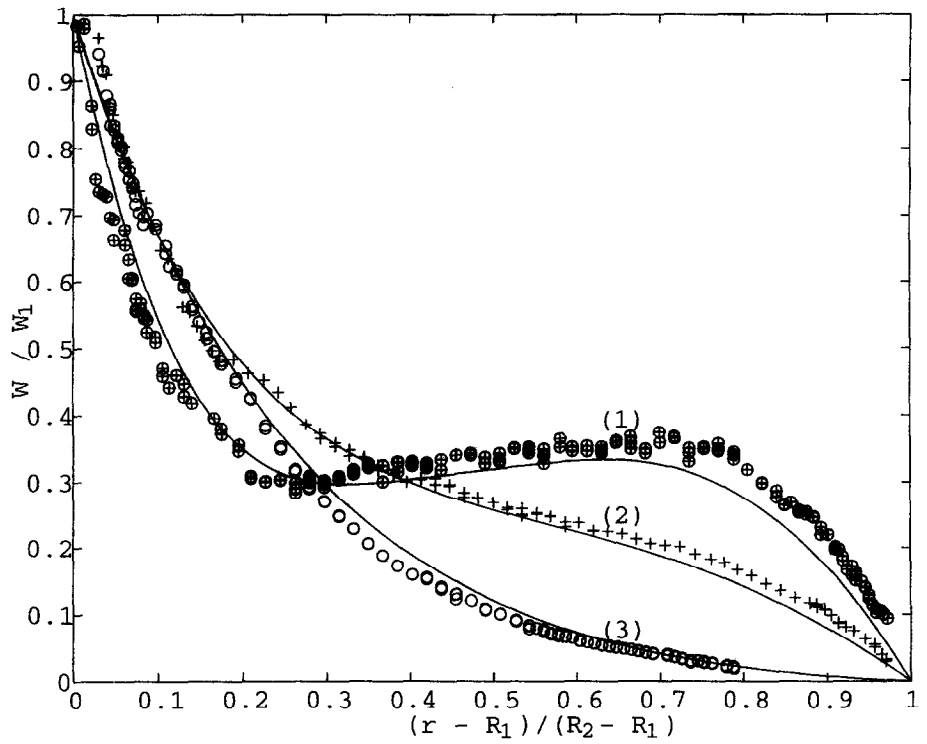

(a)

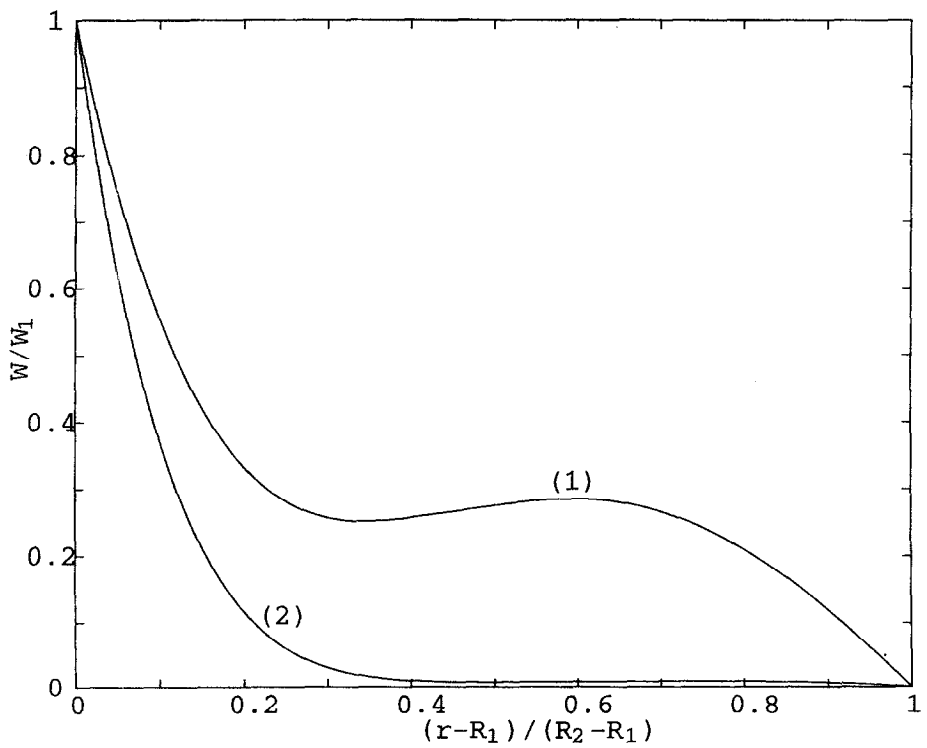

(b)

Fig. 8. – Fully developed tangential velocity profiles. (____) numerical. (1) $Qv = 1.5\,10^{-4}\,\mathrm{m^3/s}$; $\Omega_c = 2.75\,\mathrm{rd/s}$, $\Omega/\Omega_c = 1.01$; (2) $Qv = 1.5\,10^{-4}\,\mathrm{m^3/s}$, $\Omega/\Omega_c = 5.1$; (3) $Qv = 0$, $\Omega = 13.8\,\mathrm{rd/s}$; b) Fully developed tangential velocity profiles: $n = 0.5$; $\mathrm{Ro}/\mathrm{Ro}_c = 1$. (1) $ap_0 = 0.2$; (2) $ap_0 = 0.8$.

For low values of X^+ which will be specified later, the thermal boundary layer is confined to a region sufficiently close to the outer cylinder wall to enable the use of a linear velocity profile in this region: this is the Lévêque approach. Then (Bird *et al.*, 1983): $\mathrm{Nu} \propto \varphi_p^{1/3}(X^+)^{-1/3}$. The non-Newtonian behavior effect on the heat transfer can then be taken into account by a simple multiplication of the Newtonian Nusselt number, by a correction factor $\Delta^{*1/3}$. This correction factor $\Delta*$ is the ratio of the wall axial velocity gradient compared to that which would be obtained for a Newtonian fluid at the same flow rate.

$$\mathrm{Nu_{Hb}} = \Delta^{*1/3}\,\mathrm{Nu_{Newt}};\quad \Delta^* = \frac{(du/dr)_{\mathrm{Hb},r=R_2}}{(du/dr)_{\mathrm{Newt},r=R_2}}. \tag{15}$$

This method was verified experimentally for power law fluids, by Tanaka *et al.* (1974) and Joshi and Bergles (1980). The dimensionless distance X_1^+, where the Lévêque assumption and therefore the correction (15) can be applied, is determined by the following simple analysis.

In the thermal entrance region, the thickness of the thermal boundary layer $\bar{\delta}_T = \delta_T/R_2$ is $0(X^+/\varphi_p)^{1/3}\,(1-N)^{2/3}$. For a given dimensionless axial position X^+, the thermal boundary layer thickness decreases with the increase of φ_p. According to equations (14) and (15), any axial velocity profile (in the region where Lévêque hypothesis can be used), leads to the same heat transfer coefficient, provided that it has: (i) the same wall axial velocity gradient φ_p, and (ii) provides the same flow rate. On the other hand, we consider an approximation of the axial velocity profile in the sense of the norm H^1. A simple example of this approximate profile which satisfies conditions (i) and (ii), could be represented by a flat part ($U = \tilde{U}_{\max}$) in the central region of the annular space, and a linear part $U = \varphi_{p_{1,2}}\eta$, in the vicinity of the inner and outer cylinders. The conditions (i) and (ii) make it possible to calculate $\tilde{U}_{\max}$ easily. We postulate that the order of X_1^+ can be obtained using this approximate axial velocity profile. Therefore, the Lévêque assumptions cease to be valid when the thermal boundary layer reaches the flat part of the profile. After some simple calculations, we obtain:

$$X_1^+ \text{ is } 0\left(\frac{\tilde{U}_{\max}^3}{2\varphi_p^2}\,\frac{1}{(1-N)^2}\right). \tag{16}$$

The effect of the rheological behavior on X_1^+ is contained in φ_p. We find that X_1^+ diminishes with the increase of the dimensionless axial wall velocity gradient. A systematic study has been conducted for three radius ratios, $N = 0.4$, 0.5 and 0.6, and flow behavior index $n = 0.5$. It shows that for $0 \leq ap_0 \leq 0.5$ and $0 \leq \mathrm{Ro} \leq 5\mathrm{Ro}_c$, the correction (15) can be applied with a maximum relative error of 5%, in comparison with numerical analysis, when $X^+ \leq X_1^+$ given by (16).

5.2. Temperature-dependent consistency

The decrease of K close to the heated wall induces a reorganization of the flow, and modifies the heat transfer. These two points will be described through the evolution along the heating zone of the axial velocity profile, plug dimension, wall axial velocity gradient and Nusselt number. Using the dimensionless temperature $\Delta\Theta$, K can be written as $K = K_e \exp[-\mathrm{Pn}\Delta\Theta]$, where K_e is the consistency at the inlet temperature, and Pn is the Pearson number: $\mathrm{Pn} = (b\phi_p D_h)/2\lambda$.

5.2.1. *Evolution of the plug flow dimension and axial velocity profiles along the heating zone.*

First of all, recall that for the isothermal situation, when the consistency decreases, ap_0 and the critical Rossby number increase (*Fig.* 5). Consider now the situation where the fluid is uniformly heated from T_0 to T_1. Then, for a given n, N and Ro, we have (*Fig.* 9):

$$T_1 > T_0;\quad ap_0(T_1) > ap_0(T_0);\quad \mathrm{Ro}_c(T_1) > \mathrm{Ro}_c(T_0).$$

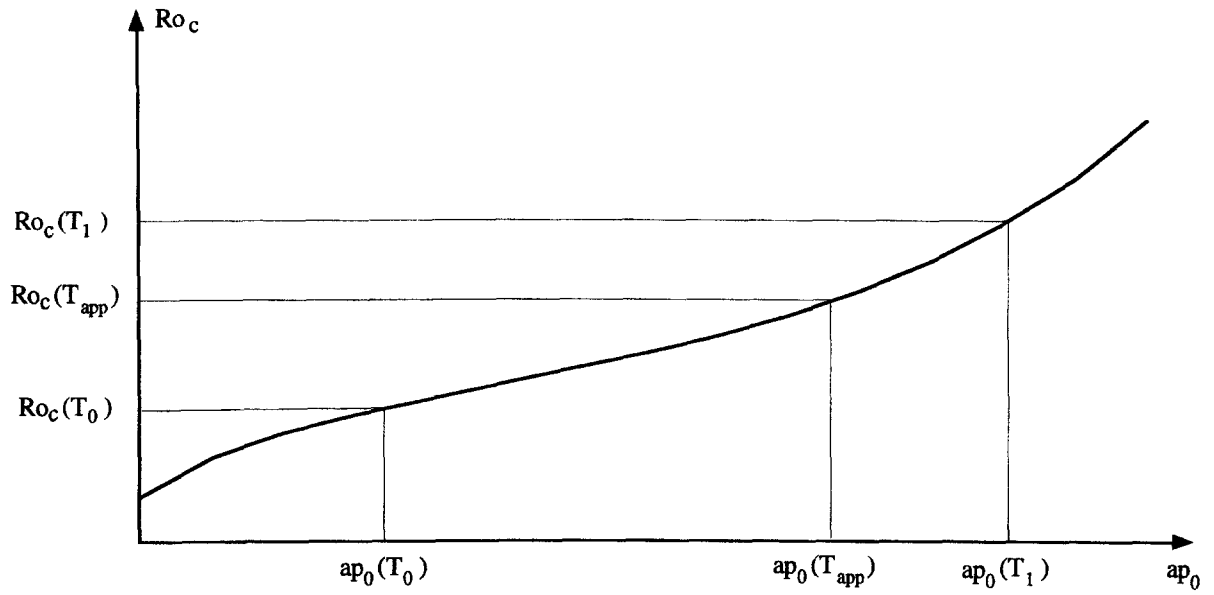

Fig. 9. – Schematic representation of the temperature effect on the plug zone width.

As far as the width ap of the plug flow is concerned, respectively at T_0 and T_1, two cases are distinguished, depending on the Rossby number (*Fig.* 9):

Case 1: $\mathrm{Ro} < \mathrm{Ro}_c(T_0)$ then $ap(T_1) > ap(T_0)$

Case 2: a) $\mathrm{Ro}_c(T_0) < \mathrm{Ro} < \mathrm{Ro}_c(T_1)$. So, $ap(T_0) = 0$ and $ap(T_1) > 0$. One can find a temperature $T_{app} : T_0 < T_{app} < T_1$, for which Ro becomes equal to $\mathrm{Ro}_c(T_{app})$, and induces the appearance of a plug flow.

b) $\mathrm{Ro} > \mathrm{Ro}_c(T_1) > \mathrm{Ro}_c(T_0)$. So, $ap(T_0) = ap(T_1) = 0$. There is no plug flow. One can say that a decrease of K favours the development of the plug flow; on the other hand, inner cylinder rotation reduces it.

Similar evolution is observed numerically in the case of non uniform heating. Figure 10 shows, the evolution of the internal and external edges of the plug flow, along the heating zone, for $n = 0.5, \mathrm{Pn} = 10$, $N = 0.5$, $ap_{0,e} = 0.4$, and for different Rossby numbers: $\mathrm{Ro} = 0$; $0.5\,\mathrm{Ro}_{c,e}$; $1.0\,\mathrm{Ro}_{c,e}$; $2\,\mathrm{Ro}_{c,e}$; $5\,\mathrm{Ro}_{c,e}$. The subscript e corresponds to the entrance section. As above, two cases are distinguished.

Case 1: $\mathrm{Ro} < \mathrm{Ro}_{c,e}$ (curves 1 and 2). We observe clearly two steps in the evolution of plug core boundaries. In the first step, under the effect of the decrease of the consistency close to the heated wall, the axial velocity gradient increases at the outer cylinder, and decreases at the inner one, due to flow rate conservation. The plug flow is radially displaced towards the heated wall, and its width increases. This deviation is more important at the external edge than that at the internal one, because the thermal boundary layer is not yet developed. In the second step, the thermal boundary layer thickens and reaches the inner cylinder. This leads to a decrease of K, and therefore, to an increase of the plug flow dimension, in the whole annular space. The wall axial velocity gradient increases at the inner cylinder and at the outer one. Consequently, the axial velocity profile tends asymptotically towards a flat profile.

From experimental point of view, Figure 11 shows two axial velocity profiles, measured before and after heating. They were obtained for $n = 0.4$, $ap_{0,e} = 0.28$, $Qv = (1.25 \pm 0.03)\,10^{-4}\ \mathrm{m}^3/\mathrm{s}$, $\Omega = 0$ and $\mathrm{Pn} = 4.55$. Theoretical profiles are represented as continuous lines. Computations took into consideration that velocities were measured 5 cm away from the heated zone. There is a good agreement between numerical and experimental results. The axial velocity profiles measured at the outlet of the heating zone correspond to the first stage of

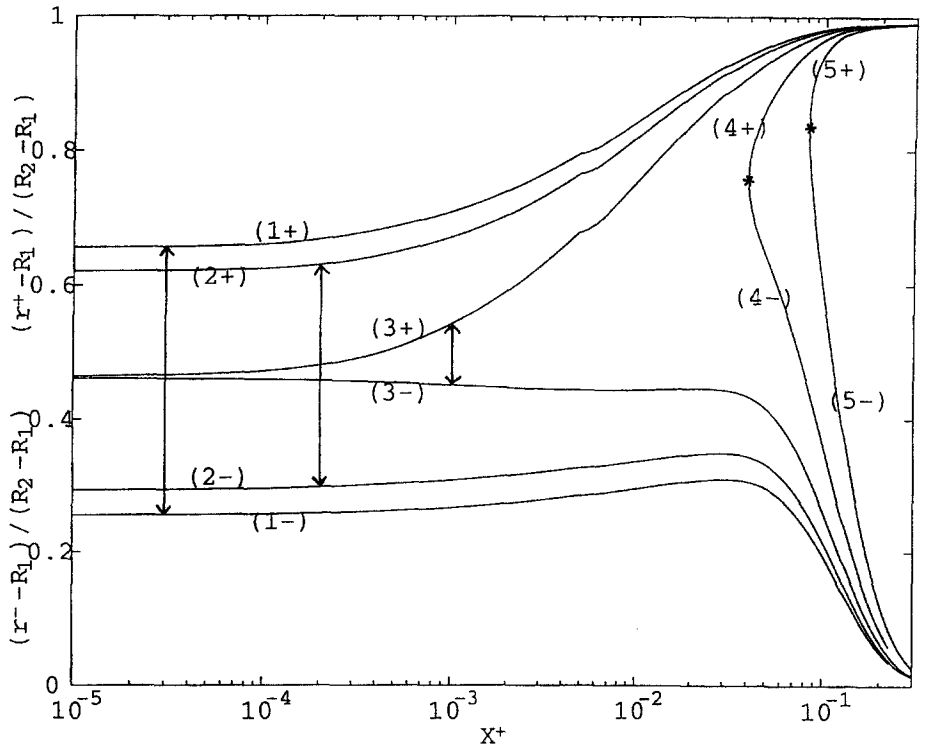

Fig. 10. – Evolution of the dimensionless outer (+) and inner (–) radius of the plug core region along the heating zone. $n = 0.5$; $\mathrm{Pn} = 10$; $ap_{0,e} = 0.4$; $N = 0.5$; (1) Ro = 0; (2) Ro = 0.5 $\mathrm{Ro}_{c,e}$; (3) Ro = 1 $\mathrm{Ro}_{c,e}$, (4) Ro = 2$\mathrm{Ro}_{c,e}$, (5) Ro = 5; $\mathrm{Ro}_{c,e}$; (*) appearance point of the plug flow.

the flow reorganization as described above. The experimental conditions (fluid used, length of the test section) did not allow observation of the second stage.

Remark 2. – The regularized model permits deformations of the "unyielded" material, whatever the stress.

Remark 3. – If we examine closely what is happening in the plug flow, we find that the radial velocity is very low $O\ (10^{-3}\ U_d)$, close to the entrance and of $O(10^{-5}U_d)$, at $X^+ = 10^{-3}$. The axial and angular velocities are considered as constant in the plug cross section, and vary weakly with the axial position. This is giving rise to a small strain rate. Therefore, when the yield criterion is applied, these areas appear to be unyielded. Walton and Bittleston (1991) found a similar region in their study of the flow of Bingham plastic, in an eccentric annulus. They termed this a pseudo-plug region, since from equation (7-b), the unyielded material is perfectly rigid. It is natural to enquire how the flow structure can evolve with distance from the entry, with an increase of the axial velocity near the heated wall, if we considered the unyielded material as perfectly rigid solid. According to Piau (1996), it is possible to study viscoplastic fluids that are elastic at low stress level. Therefore, the viscoplastic rigidity constraint is relaxed and the fluid can deform, even when the yield stress level is not reached. The question is to know whether the deformation undergone by the material, between the entrance and the exit of the heating zone, is possible with a stress level within the yield limit. In fact, Oldroyd (1947) was the first to propose that the unyielded material should be regarded as an elastic solid. The problem of the detailed coupling of a solid elastic region, to a liquid viscoplastic region, has not to the authors knowledge, received any further attention.

Case 2. – $\mathrm{Ro} > \mathrm{Ro}_{c,e}$: As it was explained before, the inner cylinder rotation and the decrease of K with temperature, have opposite effects on the plug flow dimension. Assume that we can define ap_0 and a critical

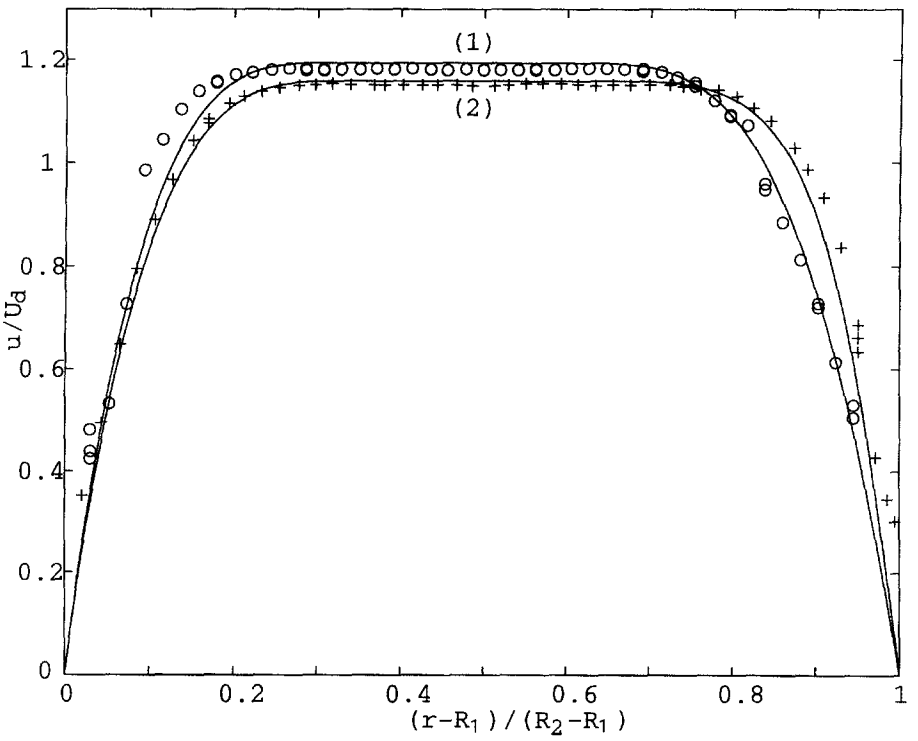

Fig. 11. – Evolution of the axial velocity profile along the heating zone: Ro = 0. Comparison between numerical and experimental results. $n = 0.4$, $ap_{0,e} = 0.28$ $Qv = 1.25\,10^{-4}$ m^3/s : (o) isothermal; (+) $\phi_p = 19850$ W/m^2 (Pn = 4.55); (____) numerical result: (1) isothermal, (2) Pn = 4.55.

Rossby number, at any axial position. From the inlet section, the fluid temperature increases along the heating zone. Consequently, $ap_0(X^+)$ and $\mathrm{Ro}_c(X^+)$ increase also. The rotating effect of the inner cylinder dominates until an axial position X_p^+: there is then no plug flow. At $X^+ = X_p^+$, the fluid temperature has increased sufficiently, so that $\mathrm{Ro} = \mathrm{Ro}_c(X_p^+)$. This leads to the appearance of plug flow at a point $P(\eta_p, X_p^+)$. Numerical results show, as it was expected, that the point (P) moves downstream and towards the heated cylinder, when Ro increases. Figure 12 shows the evolution of the radial position η_p for Pn = 10, $n = 0.5$, $ap_{0,e} = 0.4$, and for different Rossby numbers. From X_p^+, the heating effect becomes dominant . Then, the plug flow dimension increases, until it occupies practically all the annular space. The axial velocity profiles evolve in a similar way as described for case 1. Figures 13a and 13b show, as an example, the first and the second stage of the axial velocity profile evolution, along the heating zone, for $n = 0.5$; $ap_{0,e} = 0.4$; Pn = 10 and $\mathrm{Ro} = 2\mathrm{Ro}_{c,e}$. The profiles numbered (4) and (5) in the Figure 13b are shown as dashed lines, to indicate an asymptotical behavior which is difficult to reach experimentally, because it corresponds to the case of a long duct, where the wall temperature will become too high.

Furthermore, the axial pressure gradient decreases with the Rossby number and along the heating zone. If $\partial P/\partial Z$ becomes small compared to the yield stress, then numerical results show the appearance of a plug zone attached to the outer cylinder. This result is similar to that obtained by Bittleston and Hassager (1992), for an isothermal situation, with an imposed axial pressure gradient.

5.2.2. *Evolution of the wall axial velocity gradient along the heated zone*

It was shown in the paragraph 5.1 that, for an isothermal situation, the inner cylinder rotation induces a decrease of the axial velocity gradient at the outer cylinder. In the following, we examine how $(\partial u/\partial r)_2$ depends on the

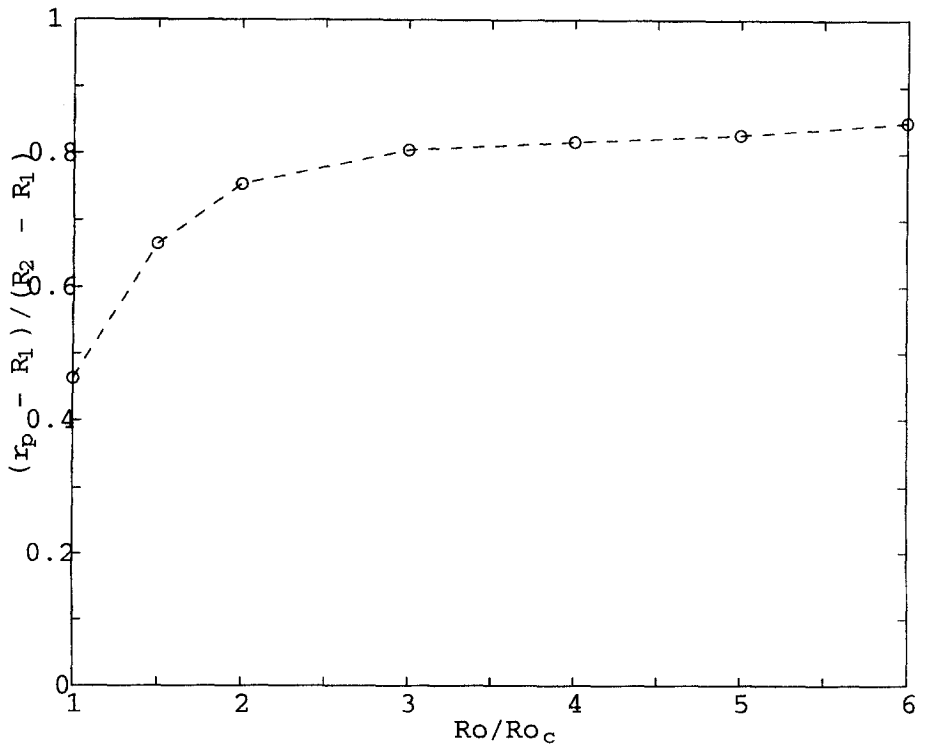

Fig. 12. – Radial position of the appearance point of the plug core as a function of $\mathrm{Ro}/\mathrm{Ro}_c$: Pn = 10, $n = 0.5$; $ap_{0,e} = 0.4$.

variation of K with temperature, for different angular velocities. Figure 14 gives $\Delta' = (\partial u/\partial r)_2/(\partial u/\partial r)_{2,z=0}$ against the axial position X^+, for $n = 0.5$, $ap_{0,e} = 0.4$, Pn = 10, $N = 0.5$ and for three Rossby numbers: $\mathrm{Ro}/\mathrm{Ro}_{c,e} = 0$; 2 and 7. It shows that axial velocity gradient increases along the heating zone. The curve (3) $(\mathrm{Ro}/\mathrm{Ro}_{c,e} = 7)$ corresponds to the case where the axial pressure gradient becomes small, compared to the yield stress. There is plug attached to the outer cylinder, and Δ' tends to 0. Near the entrance section, and for a given axial position, Δ' rises with the ratio $\mathrm{Ro}/\mathrm{Ro}_{c,e}$. This means that the thermodependence of the fluid is more apparent for higher rotating velocities. In fact, the wall temperature increases with Ro, due to the decrease of $(\partial u/\partial r)_2$ at $z = 0$. Hence, the decrease of K, and further the modification of the axial velocity profile, is more apparent. This result agrees with the experimental observations of Naïmi *et al.* (1990). In the thermal entrance region, an analytical approach of Δ' can be proposed. We consider: (i) A large Prandtl number, so that the mechanical relaxation length along the annular duct is insignificant, compared with the thermal relaxation length, that is the local velocity field adjusts almost instantaneously to the local temperature; (ii) $X^+ \ll 1$, so that temperature variations are small everywhere, except in a very thin thermal boundary layer by the outer cylinder wall. As a result, viscosity variations are not sufficiently large to cause significant variation in the pressure gradient (Ockendon *et al.*, 1977, Richardson, 1986). It then follows that the dependence of $\tau_{r,z}$ upon X^+ can be neglected. In this short entry region, we assume that the decrease of the viscosity near the heated wall is offset by the increase of the wall shear rate. This assumption was verified by solving the full problem numerically. It is also assumed that, at the wall of the outer cylinder, the tangential velocity gradient $(\partial w/\partial r - w/r)$ is small compared to the axial velocity gradient $(\partial u/\partial r)$, and can then be neglected in the second invariant D_{II}. Hence:

$$\Delta' = \frac{|\partial u/\partial r|_z}{|\partial u/\partial r|_e} \approx \left[\frac{K_e}{K(z)}\right]^{1/n} \quad \text{with} \quad K = K_c \exp[-b(T_p - T_e)]. \tag{17}$$

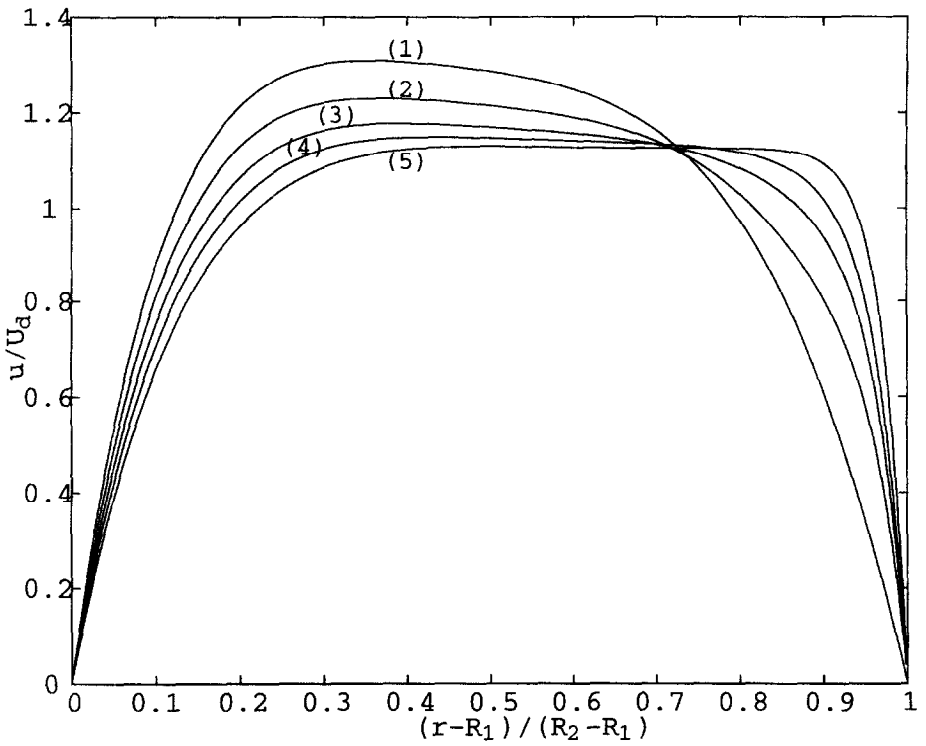

(*a*)

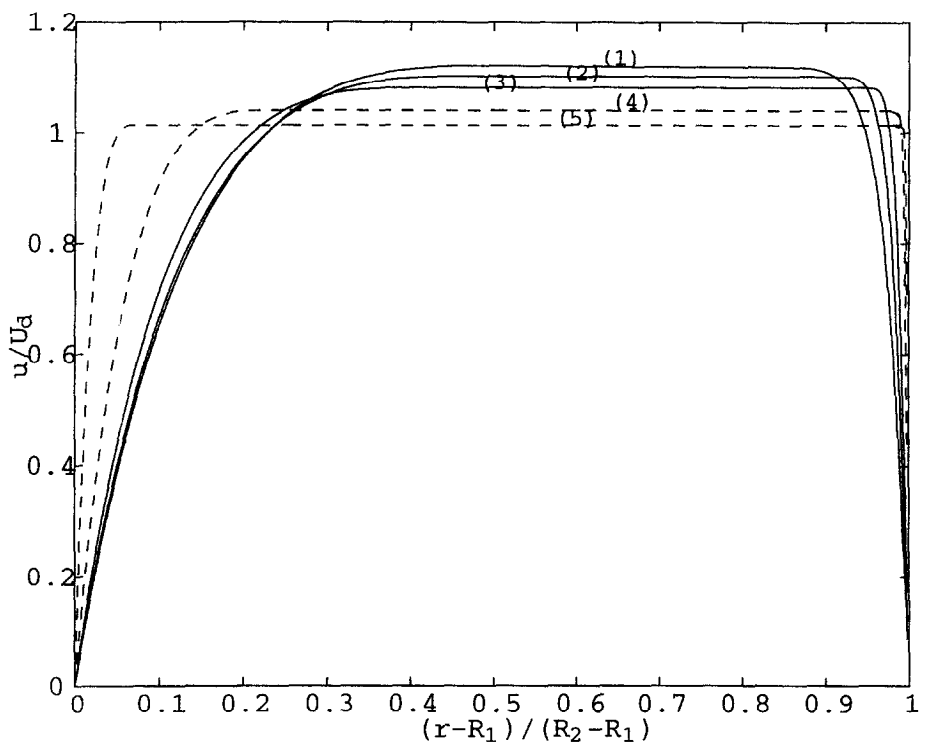

(*b*)

Fig. 13. – a) Evolution of the axial velocity profile along the heating zone: First stage. $n = 0.5$; $ap_{0,c} = 0.4$; $Ro = 2\mathrm{Ro}_c$; Pn = 10. (1) $X^+ = 0$; (2) $X^+ = 6.07\,10^{-4}$; (3) $X^+ = 2.55\,10^{-3}$; (4) $X^+ = 7.91\,10^{-3}$; (5) $X^+ = 3.04\,10^{-2}$; b) Evolution of the axial velocity profile along the heating zone: Second stage. $n = 0.5$; $ap_{0,c} = 0.4$; $Ro = 2\mathrm{Ro}_c$; Pn = 10. (1) $X^+ = 4.01\,10^{-2}$; (2) $X^+ = 5.96\,10^{-2}$; (3) $X^+ = 7.91\,10^{-2}$; (4) $X^+ = 0.13$; (5) $X^+ = 0.20$.

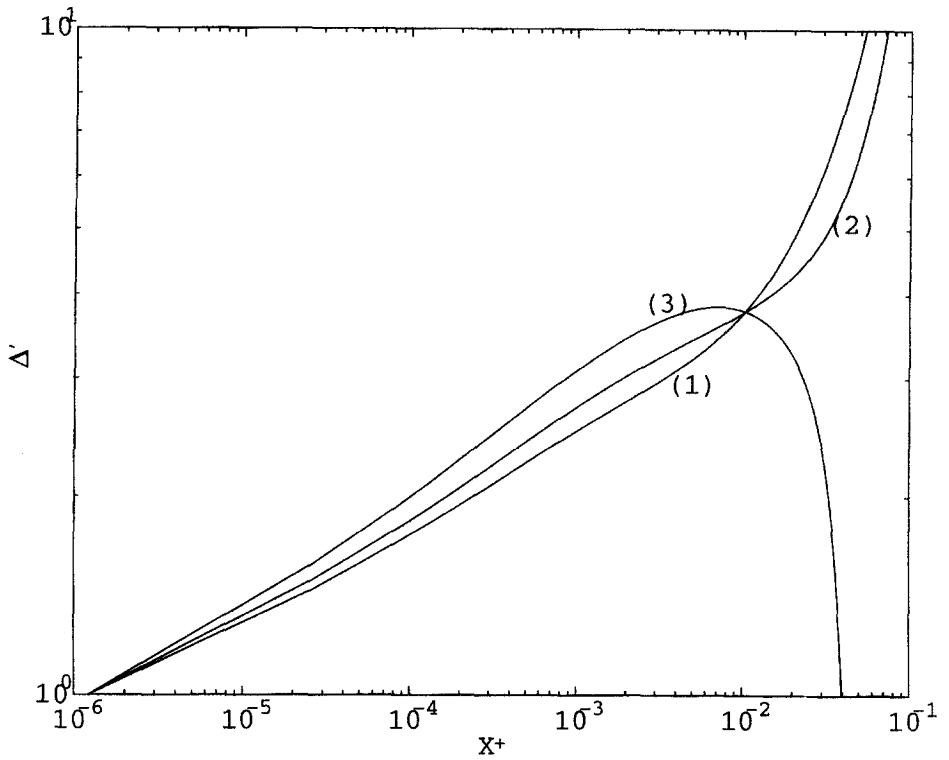

Fig. 14. – Reduced wall axial velocity gradient, $\Delta' = (\partial u/\partial r)_2/(\partial u/\partial r)_{2,z=0}$, versus Cameron number X^+ : $n = 0.5$, $ap_{0,e} = 0.4$, Pn = 10, $N = 0.5$ (1) Ro = 0; (2) Ro = $2\mathrm{Ro}_{c,e}$; (3) Ro = $7\,\mathrm{Ro}_{c,e}$.

The temperature difference (Tp-Te) is calculated to a first approximation by equation (15):

$$T_p - T_e \approx \frac{\phi_p D_h}{\lambda \Delta^{*1/3} \mathrm{Nu}_{\mathrm{new}}}. \tag{18}$$

So:

$$\Delta' \approx [\exp[\mathrm{Pn}/(\Delta^{*1/3}\mathrm{Nu}_{\mathrm{new}})]]^{1/n}. \tag{19}$$

This expression overestimates Δ', because the wall temperature is higher with constant physical properties. However, it shows clearly that for a yield stress fluid, the increase of the wall axial velocity gradient, due to the variation of consistency with temperature, is more important that Δ^* is low. In particular, when the rotational velocity increases, Δ^* decreases and therefore Δ' grows. The extent X^+, where equation (19) can be used is as large as Pn is small. In the case of a pseudoplastic fluid flow in a duct with heated wall at constant temperature, the extent of the region where $\partial p/\partial z \approx$ cste, is $O(\mathrm{Pn}^{*2}\, e^{-2\mathrm{Pn}^*})$ (Richardson, 1987), with $\mathrm{Pn}^* = n\, b\,(\mathrm{Tp} - \mathrm{Te})$.

5.2.3. *Heat transfer*

The heat transfer between the heated wall of the outer cylinder and the fluid can be examined in Figure 15a. It shows the evolution of the local Nusselt number, versus the Cameron number, in the thermal entrance region, for $n = 0.38$, $ap_{0,e} = 0.28$, $Qv = 1.46\ 10^{-4}$ m^3/s, Pn = 3.37 and for three values of Ω : 0, 14.7rad/s(Ro/Ro_c = 4.9) and 26.7rad/s(Ro/Ro_c = 8.9). In this case, $\mathrm{Ro}_c = 0.85$, Pr = $1.22\ 10^4$

and $\mathrm{Pe} = 1.25\ 10^4$. The Nusselt number decreases along the heating zone, due to the increase of thickness of the thermal boundary layer. At the end of the heating zone, δ_T is about 2.8 mm for $\Omega = 0$ and about 3.15 mm for $\Omega = 26.7$ rad/s. For a given axial position, the inner cylinder rotation reduces $(\partial u/\partial r)_2$, thereby reducing the Nusselt number. The difference between the experimental and the numerical results, represented by a continuous line, is less than 5%.

Remark 4. – For all the experimental tests, the temperature difference between the top and the bottom of the outer cylinder did not exceed 1°C. Thus, the free convection effect is weak and can be neglected. Forced convection remains the dominant mechanism governing the heat transfer to the fluid.

Figure 15b shows a classical result, relative to the increase of the Nusselt number with the Pearson number. Experimentally, the effect of the temperature dependent fluid consistency on heat transfer is not very well marked. This is because, the fluid used is slightly thermodependent and also because there is a gradual increase of the outer cylinder temperature, when it is subjected to a constant heat flux.

Remark 5. – The numerical calculations show that the Nusselt number tends asymptotically towards

$$\mathrm{Nu}_\infty = \frac{2(1-N)^2(1+N)}{\frac{1-3N^2}{4} - \frac{N^4\mathrm{Log}(N)}{1-3N^2}}.$$

This value is due to the flat asymptotic axial velocity profile.

To obtain a Nusselt number correlation in the thermal entry region, an extension of the Lévêque method is used. Combining the modification of the wall axial velocity gradient due to the non-Newtonian behavior, and the variation of the consistency with temperature, we can write:

$$\varphi_p = \varphi_{p,vk} = \frac{\varphi_{p,ck}}{\varphi_{p,\mathrm{New}}} \cdot \frac{\varphi_{p,vk}}{\varphi_{p,ck}} \cdot \varphi_{p,New} = \Delta^* \cdot \Delta' \varphi_{p,\mathrm{New}} \tag{20}$$

Where the subscripts ck and vk mean respectively, constant and variable consistency and Δ' represents the modification of the wall axial velocity gradient, due to the decrease of the consistency with temperature.

The Nusselt number can then be written as follows:

$$\mathrm{Nu} = 1.034(1-N)^{1/3} \varphi_{p,\mathrm{New}^{1/3}} \left(\frac{X^+}{\Delta^* \Delta'}\right)^{-1/3}. \tag{21}$$

If Δ' is replaced by equation (19), then the expression (21) describes the numerical results perfectly for $10^{-6} \leq X^+ \leq 10^{-4}$. For increasing X^+, the equation (21) overestimates the Nusselt number and departs progressively from that obtained numerically. In fact, Δ' was determined in the short entry region where $\partial p/\partial z$ is constant, and in paragraph, 5.2.2 it was explained that equation (19) overestimates Δ'. Nevertheless, the numerical results show that for a large range of X^+, the Nusselt number evolution can be written as:

$$\mathrm{Nu} = A(X^+)^B \tag{22}$$

where A and B are identified using relations (21) and (22) in the short entry region, B being given by $B = -\frac{1}{3} + \frac{\mathrm{Pn}}{3\Delta^{*1/3}\mathrm{Nu}_{\mathrm{New}}}$.

Here, A and B are replaced by their average values for $10^{-6} \leq X^+ \leq 10^{-4}$. The expression (22) was then checked numerically for $0.4 < N < 0.6$; $0 < ap_{0,e} < 0.5$; $0.3 < n < 0.8$; $0 \leq \mathrm{Pn} \leq 10$; $0 < \mathrm{Ro} < 5\mathrm{Ro}_{c,e}$ and $10^{-5} < X^+ < X_1^+$. The maximum difference between numerical results and the correlation (22) is 10%. From the experimental point of view, Figure 16 shows the ratio of the experimental Nusselt number to the

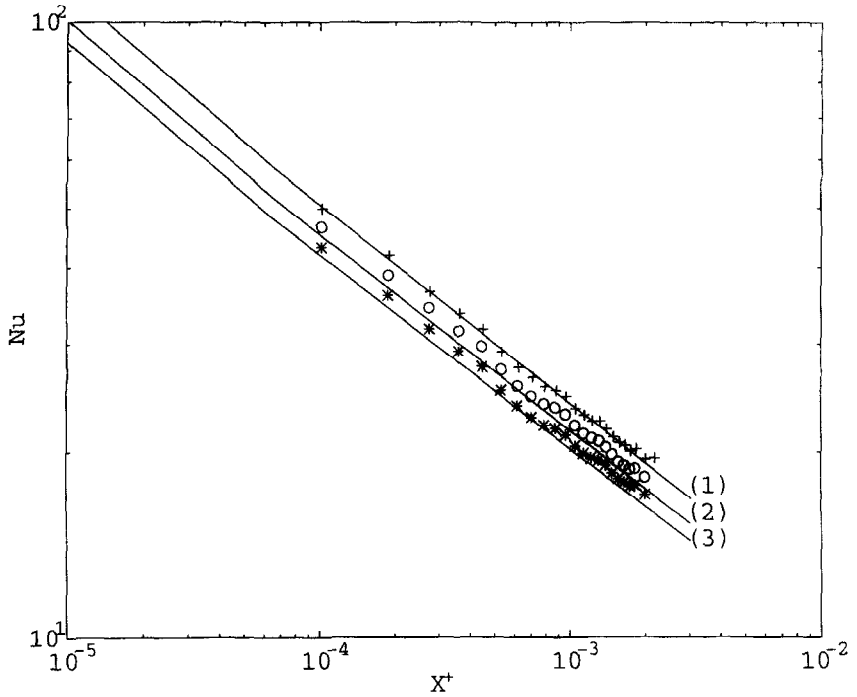

(a)

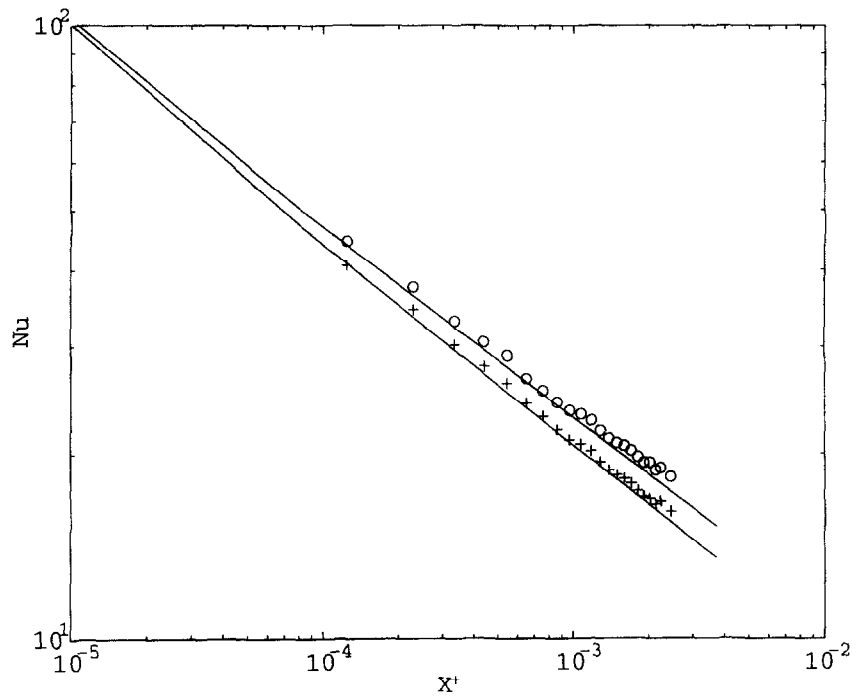

(b)

Fig. 15. –

Fig. 15. – a) Evolution of the local Nusselt number along the heating zone. $n = 0.38$, $ap_{0,c} = 0.28$, $Qv = 1.46\,10^{-4}\,\mathrm{m^3/s}$, $\phi_p = 14700\,\mathrm{W/m^2}$; $\mathrm{Pn} = 3.37$; $\Omega_c = 3.0\,\mathrm{rad/s}$; (+) $\Omega = 0$; (o) $\Omega = 4.9\,\Omega_c$; (*) $\Omega = 8.9\,\Omega_c$; (____) numerical prediction; b) Evolution of the local Nusselt number along the heating zone. $n = 0.40$, $ap_{0,c} = 0.28$, $Qv = 1.25\,10^{-4}\,\mathrm{m^3/s}$, $\Omega_c = 2.57\mathrm{rad/s}$; $\Omega = 4.07\Omega_c$; (+) $\phi_p = 22600\,\mathrm{W/m^2}$ ($\mathrm{Pn} = 5.18$); (o) $\phi_p = 7630\,\mathrm{W/m^2}$ ($\mathrm{Pn} = 1.75$); (____) numerical prediction.

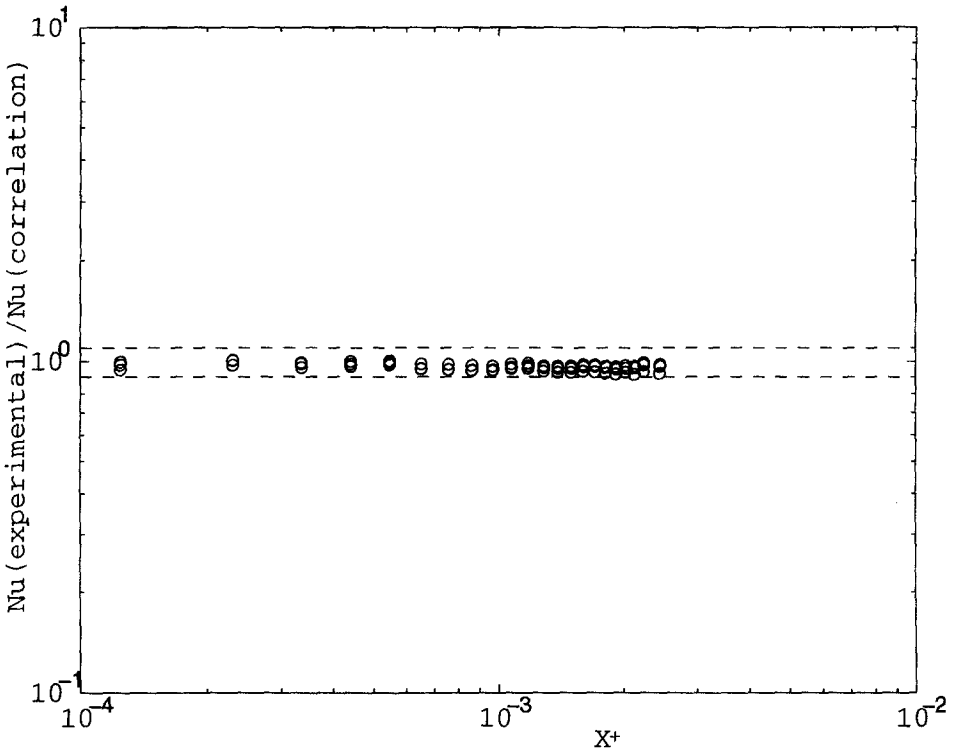

Fig. 16. – Comparison of experimental results (circle) with correlation, (- - - - -) ±10% scatter band.

Nusselt number obtained by equation (22). Once again, the maximum deviation of the experimental results from the correlation is 10%.

Remark 6. – In the situation where there is a plug core attached to the outer cylinder, the wall temperature increases sharply and therefore the heat transfer coefficient is strongly reduced.

6. Conclusion

The characteristics of the thermal convection, for a Herschel-Bulkley fluid flowing in an annular duct, with rotating inner cylinder, have been investigated numerically and experimentally. In order to discern the effect of non-Newtonian behavior from that attributable to temperature-dependent consistency on the flow field and heat transfer, a study with constant consistency was first performed. For fully developed dynamic regime, the critical Rossby number Ro_c, above which, the plug core is reduced to zero, was determined. A diagram relating Ro_c to the radius ratio N and the relative dimension ap_0 of the plug core for Poiseuille flow, has been established.

The rotation of the inner cylinder induces a decrease of the axial velocity gradient $(\partial u/\partial r)$ at the outer one, and the heat transfer is then reduced. Based on the Lévêque approach, the Nusselt number is obtained by a simple multiplication of the Newtonian Nusselt number by $\Delta^{*1/3}$, where Δ^* is the ratio of the wall axial velocity gradient to that which would be obtained for a Newtonian fluid at the same flow rate. We propose a simple expression for the order of magnitude of X^+ where this approach can be applied.

The variation of K with temperature leads to a reorganization of the flow, which modifies the heat transfer between the heated wall and the fluid. This reorganization of the flow is described in the following cases. (i) If $\mathrm{Ro} < \mathrm{Ro}_{c,e}$ the dimension of the plug flow increases along the heating zone, until it occupies practically the

whole annular space. The axial velocity profiles evolve in two stages. In the first stage, $(\partial u/\partial r)$ increases at the outer cylinder and decrease at the inner one. In the second stage, $(\partial u/\partial r)$ increases at the inner and outer cylinders. The axial velocity profile tends asymptotically towards a flat profile. If (ii) $\mathrm{Ro} > \mathrm{Ro}_{c,e}$ there is no plug zone at the inlet section. The decrease of the K with temperature leads to a reappearance of the plug flow at a point (P) in the annular space, which coordinates depend on the Rossby and Pearson numbers. The dimension of the plug flow increases thereafter from (P) to occupy practically all the annular space. The axial velocity profile evolves in a similar way as for (i). If $\partial p/\partial z$ becomes small, compared to the yield stress, then the numerical results predict a plug core attached to the outer cylinder.

In the thermal entrance region ($X^+ \ll 1$), and for large Prandtl number, the modification of $(\partial u/\partial r)_2$, due to decrease of K close to the heated wall, can be appoximated by a simple analytical expression. It shows clearly that the effect of thermodependency of K on the heat transfer is more important with increasing angular velocity. Finally, this expression is used for a Nusselt number correlation.

Acknowledgments

The authors are indebted to J. P. Brancher, D. Bernardin and A. Cheikhi for fruitful discussions.

REFERENCES

ALAIN M., 1973, Le Carbopol 940: Caractérisation physico-chimique et processus de gélification, Thèse de Doctorat de l'Université de Montpellier I, Faculté de Pharmacie, France.

BERCOVIER M., ENGELMAN M., 1980. A finite element method for incompressible non-Newtonian flows, *J. Comp. Physics*, **36**, 313–326.

BERIS A. N., TSAMOPOULOS R. C., ARMSTRONG R. C., BROWN R. A., 1985, Creeping motion of a sphere through a Bingham plastic, *J. Fluid. Mech.*, **158**, 219–244.

BITTLESTON S. H., HASSAGER O., 1992, Flow of viscoplastic fluids in a rotating concentrating annulus, *J. Non-Newtonian Fluid Mech.*, **42**, 19–36.

BIRD B., DAI G. C., YARUSSO B. J., 1983, The rheology and flow of viscoplastic materials, *Rev. Chem. Eng.*, **1**, 1-110.

EL-SHAARAWI M. A. I., SARHAN A., 1982, Combined forced-free laminar convection in the entry region of a vertical annulus with a rotating inner cylinder, *Int. J. Heat Mass Transfer.*, **25**, 175-186.

FORDHAM E. J., BITTLESTON S. H., TEHRANI M. A., 1991, Viscoplastic flow in concentric annuli, pipes and slots, *Ind. Eng. Chem. Res.*, **30**, 517–524.

FORREST G., WILKINSON W. L., 1973, Laminar heat transfer to temperature-dependent Bingham fluids in tubes, *Int. J. Heat Mass Transfer.*, **16**, 2377–2391.

JOSHI S., BERGLES A. E., 1980, Experimental study of laminar heat transfer to in-tube flow of non-Newtonian fluids, *J. Heat Transfer (Trans ASME)*, **102**, 397–401.

MAGNIN A., PIAU J. M., 1987, Shear rheometry of fluids with a yield stress, *J. Non-Newtonian Fluid Mech.*, **23**, 91–106.

NAIMI M., DEVIENNE R., LEBOUCHE M., 1990, Étude dynamique et thermique de l'écoulement de Couette-Taylor-Poiseuille : Cas d'un liquide présentant un seuil d'écoulement, *Int. J. Heat Mass Transfer.*, **33**, 381–391.

NOUAR C., DEVIENNE R., LEBOUCHE M., 1987, Convection thermique pour l'écoulement de Couette avec débit axial; cas d'un fluide pseudoplastique, *Int. J. Heat Mass Transfer.*, **30**, 639–647.

NOUAR C., LEBOUCHE M., 1996, Thermal convection for a thermodependent Herschel-Bulkley fluid in an annular duct, Heat and Mass Transfer, **31**, 257–267.

OCKENDON H., OCKENDON J. R., 1997, Variable viscosity flows in heated and cooled channels, *J. Fluid. Mech.*, **83**, 177–190.

OLDROYD J. G., 1947, A rational formulation of the equations of plastic flow for a Bingham solid, *Proc. Camb. Philos. Soc.*, **43**, 100–105.

PIAU J. M., 1996, Flow of a yield stress in a long domain. Application to flow on an inclined plane, *J. Rheology.*, **40**, 711–723.

RICHARDSON S. M., 1986, Flows of variable viscosity fluids in ducts with heated walls, *Journal of Non-Newtonian Fluid Mech.*, **25**, 137–156.

ROUND G. F., YU S., 1993, Entrance laminar flows of viscoplastic fluids in concentric annuli, *Can. J. Chem. Engng.*, **71**, 642–645.

TANAKA M., MITSUICHI N., 1974, Non-newtonian laminar heat transfer in concentric annuli, *Kagaku-Kogaku.*, **38**, 664–671.

WALTON J. C., BITTLESTON J., 1991, The axial flow of a Bingham plastic in a narrow eccentric annulus, *J. Fluid Mech.*, **222**, 39–60.

WORSOE-SCHMIDT A. E., 1967, Heat transfer in the thermal entrance region of circular tubes and annular passages with fully developed laminar flow, *Int. J. Heat Mass Transfer*, **10**, 541–551.

(Manuscript received October 13, 1997;
accepted January 1, 1998.)